Fall 2016

Distributed fiber-optic temperature sensor validations using field deployments in the flooded Orphan Boy mine shaft in Butte, MT

Elliott Mazur
Montana Tech

Master's Research Project Summary
Distributed fiber-optic temperature sensor validations
using field deployments in the flooded Orphan Boy mine shaft in Butte, MT

By: Elliott Mazur, M.S. Candidate in Geoscience

Abstract

The process of sensor validation through experimentation with the Omnisens Distributed Temperature and Strain (DITEST) Brillouin Optical Time Domain Analyzer (BOTDA) proved to be a challenging project. The project encompassed sensor calibrations, system error minimization, sensor network design and deployment, and the characterization of temperatures in the Orphan Boy Mine shaft. Fiber-optic cable sensor calibrations yielded linear relationship coefficients 0.6-1.0MHZ/°F, indicating a strong positive correlation between Brillouin Frequency Shifts and temperature. Calibrated sensors demonstrated accuracies near ±0.8°F using the corrected error bounds from residual analyses as the benchmark. Fiber-optic measurement accuracy and repeatability were controlled by user-selected signal interrogator settings and design limitations within the system.

Temperatures monitored during the February-July 2016 period showed little variation except when the Geothermal Heat Exchange System was in operation. A test of the geothermal system (used to heat the Natural Resources Building on the Montana Tech campus) was documented by the fiber-optic sensor cluster deployed in this project and separately by a temperature transducer from the Montana Bureau of Mines and Geology. Temperature was an auxiliary sensing function of the DITEST; temperature profiles recorded in time and depth demonstrated the capability of the Brillouin-based signal interrogator when used primarily as a temperature sensing system.

Table of Contents

Introduction

Electrical and digital sensors have been in common use for decades, giving them distinct advantages over emerging technologies like fiber-optic sensing systems. Dr. Mary MacLaughlin of Montana Tech and Dr. Herb Wang of the University of Wisconsin-Madison proposed a research project to validate the temperature, strain, and temperature measurements collected using a Brillouin-based fiber-optic signal interrogator. The research grant was accepted and approved for funding by the Centers for Disease Control (CDC) National Institute for Occupational Safety and Health (NIOSH) Mine Safety Research Division. The author joined the research team and was tasked with characterizing and validating fiber-optic responses to temperature changes using the project's primary instrument, a signal interrogator made by Omnisens, Switzerland. The Omnisens DITEST STA-R Series Brillouin Optical Time-Domain Analyzer (BOTDA) Distributed Strain and Temperature sensing (DST) instrument used a looped-fiber configuration of single-mode fiber-optic cable to measure the *Brillouin frequency shift* (BFS) in laser light passing through the fiber. The project objective was to use the fiber-optic sensors attached to the DITEST to record temperature profiles in the flooded Orphan Boy Mineshaft, thus validating the temperature-sensing capabilities of the DST.

Fiber-optic Theory

The looped cable configuration utilized by the DITEST measures and resolves BFS by sending pulses of light simultaneously from either end of the fiber loop. One side (the "pump") stimulates the BFS and the other (the "probe") identifies the measurement location. Consequently, only the half of the fiber along which the probe light-pulse travels after arrival of the pump serves as the sensor (Bao et al., 1993). Changes in the characteristics of propagating laser light can be correlated to temperature fluctuations or strain events from cable geometry alterations. DST systems are primarily strain-sensing systems, with temperature sensing as an auxiliary feature. By contrast, many Distributed Temperature Sensing (DTS) systems use Raman methods to detect temperature changes as shifts in laser light intensity ("amplitude") using multi-mode fiber-optic cables (Perez-Herrera and Lopez-Amo, 2013).

A "scan" refers to the collection of measurements at all available fiber positions for a given sensor at a given date and time. The spacing between measurement positions, referred to as "sampling points," governs spatial data resolution and is user-defined. A combination of the scan duration and the assigned time delay between consecutive scans controls temporal resolution (Glisic and Inaudi, 2008). Published literature was reviewed for additional information on optical sensing methods, the field-use of fiber-optic sensors, and the operational parameters that govern the use of distributed optical sensors.

Proofs of Concept and Case Studies

Raman-based sensing methods have been in field-use for some time, utilizing intensity-based DTS signal interrogators. Past studies range from borehole temperature monitoring (Hurtig et al., 1997), measuring thermal components of a creek (Boughton et al., 2012), monitoring groundwater influx (Bolognini and Hartog, 2013), studying Antarctic waters (Tyler et al., 2013), and observing highly sensitive shallow habitats (Hausner et al., 2013). A study by Aminossadati et al. (2010) in an underground environment assessed the performance of a Raman-based DTS for monitoring mine ventilation temperatures. Under the right conditions and with adequate scan duration, system performance approached ± 0.54°F accuracy over varying ranges, with a

common 1-meter spatial resolution. The Brillouin-based Omnisens DITEST was compared to these benchmarks to assess its viability as a temperature-sensing instrument.

Brillouin-based sensing has developed steadily over the past 25 years. Beginning with Kurashima et al. (1990), an accuracy of ±3°C and a spatial resolution of 100m with limited range (1.2 km) were possible using specially manufactured fibers. The Brillouin-based DTS unit used by Zhou et al. (2013) indicated ±1.2°C accuracy and 0.5-m spatial resolution. Lab-based experimentation was prevalent in the literature reviewed, with few assessments performed in the field such as the study Selker et al. (2006) for monitoring hydrologic systems. The author is unaware of any studies that use Brillouin sensing methods and a multi-purpose DST unit like the Omnisens DITEST to monitor temperatures in an underground environment.

Raman-based signal interrogators are limited by the transmission strength of intensity-based measurements. The DITEST has a longer sensing range (69km or greater) relative to Raman-based intensity-domain interrogation systems (1-10km) because of the frequency-domain's higher optical efficiency, or "budget". Brillouin-based systems use the frequency domain to measure temperatures, using a smaller portion of the total optical budget and allowing the system to reach farther than Raman-type intensity-based systems using the same optical budget (Kurashima et al., 1990). Once the measurement signal reaches beyond 10km, most commercially available Raman systems can no longer detect backscattered light because the intensity is below the threshold of the interrogator hardware. Published studies emphasized favor for Raman sensing methods over Brillouin sensing methods because of the improved accuracy near ±0.5°F, compared to Brillouin accuracies greater than ±1.0°F.

Pros and Cons of fiber-optic sensors and systems

Conventional methods of instrumentation use discrete sensor arrays to mimic distributed-sensor spatial coverage, but are expensive for similar coverage and require individual access for data retrieval. The term "distributed sensors" refers to sensors that utilize a single elongated body and collect data at intervals along the sensor. Specially manufactured fiber-optic cables are among the distributed sensor family and have the potential to detect changes in the intensity, frequency, scattering, and absorption of light passing through the fibers with the help of a signal interrogator.

Advantages of optical fiber sensors are their immunity to electronic and magnetic interference, immunity to measurement drift, light-speed data transmission over great distances, measurement sensitivity, and a minute deployment footprint (Hurtig et al., 1997). Temporal resolution is controlled by the size of the sensor network and by signal interrogator hardware limitations; the spatial resolution is controlled by scan duration, sensor length, sensor resolution, and the scan computation delays known as "signal resolution time" (Kurashima et al., 1990). Current technology is reducing spatial resolution differences between Raman and Brillouin systems, while temporal resolutions remain user-specified.

Distributed sensing systems like fiber-optic sensor networks are particularly useful for monitoring structures or environments whose failures are potentially hazardous to human life or significant economic impact. Overland oil pipeline monitoring, road stability monitoring in remote areas, and rock deformation monitoring in underground mining operations are a few such examples. Hazardous environments like underground mining operations require additional precautions to prevent sensor damage due to heavy equipment or material kinking or impacting the sensor body. Monitoring projects in high-hazard environments benefit from the near-real-time reporting capabilities of the nerve-like fiber-optic sensor networks, reacting to measurement

anomalies with automated operator alarms to alert equipment and personnel of the danger. Automated alarms and near-real time data processing are traits lost on most discrete sensor networks due to individual data retrieval requirements and time delays introduced by batch processing. Thus, return-on-investment for long-term or high-risk projects is better with fiber-optic sensors.

The main disadvantage of fiber-optic sensing is the high cost of signal interrogators (on average greater than $50,000) and sensor cables (on average $3-12/meter). Transmission distances add to the length of the required sensor cable, increasing cost without producing useful data. The steep learning curve of in-house cable splicing or the high cost of manufacturer splices (sometimes more than $1,300 per termination on specialized cables) prevents companies with major budget limitations from considering fiber-optic sensor networks viable in favor of less-expensive alternatives.

Challenges regarding signal transmission (forming a closed-loop) and deployment designs and complicated software manipulation introduce another steep learning curve. Delays between purchasing a system and the deployment of sensors can lead those with strict project deadlines to choose monitoring methods with shorter instrument training periods. Documentation on sensor deployment methodology is also lacking, requiring monitoring personnel to either hire a knowledgeable consultant or become their own troubleshooting group.

Lastly, cable sensors are fragile, requiring armoring (which may cause the sensor to be less sensitive to the target variable) or the placement of the sensor away from potential kinking/impact/snagging hazards (which may move the sensor away from the monitoring target, such as a wall or ventilation shaft). Using a silica fiber as a light transmission medium is effective, but prone to damage and interference at termination ends from dust.

The disadvantages described can be overcome with an appropriate budget of both funds and training time, producing clever deployment designs, a reduction of hazards to the cable, and system functionality workarounds.

Sensor best practices

Optical sensors require a more rigorous maintenance regime than traditional sensors because the detection mechanism and signal transmission medium are one-in-the-same. Fiber-optic sensors experience damage most often from impact- or bending related incidents. Maintaining minimal operational bend radii during splicing and installation and protecting from kinking, crushing, and over-straining minimize the potential for physical sensor damage.

By contrast, a fiber-optic sensor also experiences environmental contamination in the form of particulate matter on the optical connections that cause signal-reading errors by the signal interrogator. Sensor connection areas were cleaned and a closed-loop connection was maintained in all sensors to reduce the potential for system and measurement errors. Proper sensor hygiene removed cable terminations from sources of particulate (tables, the floor, the ground, etc.); termination ends/connection junctions were cleaned with optical lab-grade cleaning wipes and a particulate-free cleaning solution (pure-grade rubbing alcohol). In this manner, signal errors and failures to resolve measurement scans were minimized during all project operations.

The physical properties of the fiber-optic cable sensors chosen for this project are summarized in Table I.

Table I: Physical cable properties and mechanical limitations

Cable Parameters							
Parameter	**Brand**	**Name**	**Fiber Sets**	**Cable Makeup**	**Nominal OD**	**Minimum Operational Bend Radius**	**Operational Temp range**
Strain	Brugg	Brusens v9	1 SM*	Bonded core	3.2mm	4.8cm	-30°C to 70°C
	OCC	Mil-Tac	2 SM, 2 MM*	Core-locked, tight-buffered	4.5mm	5.5cm	-55°C to 85°C
Temperature	Brugg	Temp-85	4 SM	Armored, metal wrapped, loose-core	3.5mm	1.5cm	-40°C to 85°C
	Corning	Freedm	2 SM, 2 MM	Armored, non-metallic armoring, loose-core	9.7mm	9.7cm	-40°C to 70°C
Lead-in [signal transmission, no associated variable]	Corning	Simplex 3.0	1 SM	loose-tube core	3.0mm	1.0cm	-20°C to 70°C
* SM = Single Mode, MM = Multimode							

Appendix I details the splicing procedures common to these cables and Appendix II provides the technical specifications for each cable brand and model.

Calibration studies

System design governed calibration practices throughout the literature, though most authors did not report any calibration details. An example of a Raman-DTS calibration found in the User Manual for a SensorTran Astra5k system (2009) used fixed temperature calibration baths to match the difference in light intensity to the temperature difference between the baths. A study by Boughton et al. (2012) used an ice-water bath and a temperature logger; the correlation between temperature and optical intensity was not explained. By contrast, Brillouin-sensing studies such as those by Mizuno et al. (2015) use a range of temperatures to generate temperature-dependence coefficients from regression models, suggesting a transient or step-wise calibration setup.

Field Site

The Underground Mining Education Center (UMEC) located on the Montana Tech campus contains the Orphan Boy Mine shaft (OBM) and provides access to the Orphan Girl Mine shaft (OGM). The shafts provide a convenient field site for investigating field performance of the DITEST for documenting temperature fluctuations in water to ~80m depth and in air along the cable path to the shafts, both at 0.1m measurement intervals.

Past temperature research within the two selected mine shafts has been sparse. Gammons et al. (2009) documented mine-water chemistry, temperature, and particle flows in the OBM but did not acquire spatially-distributed temperature data. Hagan (2015) collected temperature profiles in several mineshafts in the Summit Valley Mining District; however, no spatially and temporally-continuous temperature record exists for either of the OBM or OGM. This project produced a time-series record of temperatures in the Orphan Boy Mineshaft for a 5-month period to characterize thermal variations during that period. Figure 1 shows the approximate location of the Orphan Boy and Orphan Girl Mines in relation to the ground surface west of Montana Tech. The GWIC Well 4822 is the Orphan Boy shaft (GPS location.

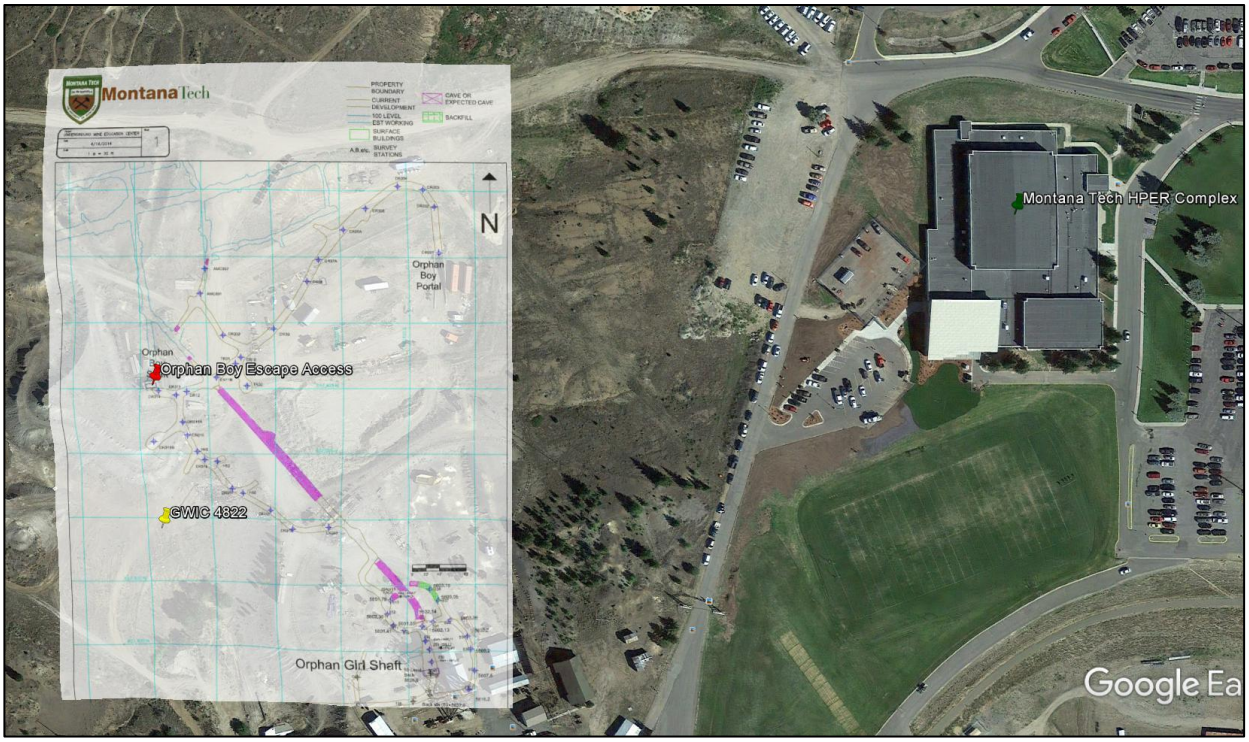

Figure 1: A map of the field site and its location relative to the western side of the Montana Tech campus. Note, the GWIC well is the steel casing that is the Orphan Boy Mineshaft; the Orphan Boy Mine is open on the 100-level as part of UMEC.

Research Objective

The primary objective of this study was to monitor mine-water temperatures as a function of position and time, providing time-series temperature profiles of the selected mine shaft and thereby validating the capabilities of the DST. The following methods were formulated to achieve the primary research objective:

- Derive sensor BFS dependency on temperature on a representative section of each brand of fiber-optic cable
- Validate calibrated sensor precision and accuracy in a controlled laboratory setting
- Deploy DST sensors in the OBM in the UMEC, log temperature profiles, document temperature fluctuations

Methods

A brief review of available literature showed that Brillouin-based systems were not in common use, nor were the calibration practices detailed in the examined studies. As a result, a small-bath/small-cable-section calibration setup was pursued as recommended by a consultant from Silixa Ltd, Thomas Coleman. Step-wise heating of the bath was not used to document quick equilibration by the fiber-optic cables because the scan duration of about 60-120 seconds would smooth-over temperature changes sensed in the 10-second range. Mr. Coleman indicated that cables with a metallic component often have equilibration times faster than the interrogator system would be able to read (Personal Communication, 31 August 2015).

Calibrations used a heated water bath and a representative section of each sensor, about 2-4m, using the 0.1m spatial resolution setting. A Coleman 48-quart cooler contained the

calibration water bath, with cold tap water heated monotonically 60-90°F by an Aqueon Pro 150 precision aquarium heating-element and circulated by a Profile 1000 aquarium air pump to prevent temperature stratification. The DITEST user manual recommended sensor cable calibrations in two temperature regimes, one from 0-20°C (32-68°F) and the other in the 20-40°C (68-104°F) range, when applicable. Cables were calibrated in the 60-90°F range as lab equipment allowed for deployment in the geothermally heated waters in the OBM & OGM. Air temperature variation in the lab was small (compared to the temperature range in the calibration bath gradient) 70.0 ± 1.5°F.

The cable coil and aquarium heater were placed horizontally in the same plane in an attempt to achieve even heating along the submerged cable coil. One TidBit placed above the cooler measured the ambient air-temperature in the room and another TidBit measured the calibration bath water-temperature, both measuring at 5-minute intervals. The calibration vessel shown in Figure 2 demonstrates the cable placement.

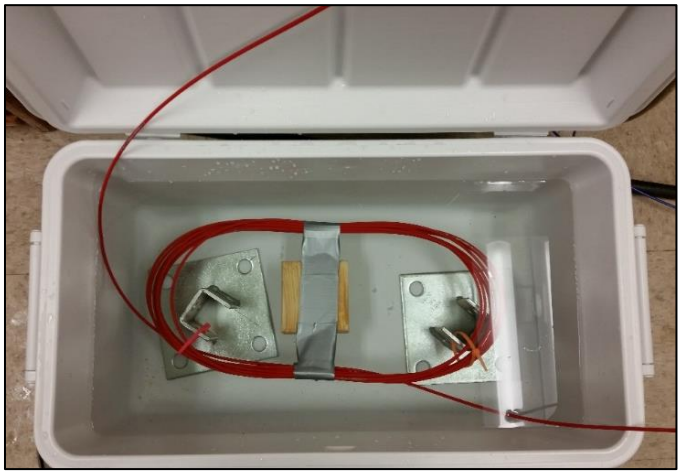

Figure 2: Experimental layout of each temperature calibration; a TidBit temperature logger placed on the wooden block suspended in the center of the coil provided a representative temperature measurement at the same depth as the cable. The aquarium pump was placed beneath the wooden block, and the heating unit was attached horizontally near the water surface, parallel to the long side of the cable coil.

Two zones were assigned along the length of the sensor cable to target the in-air and submerged sections of cable; in-air data were not used, as air temperatures were not regulated during calibrations. Most fiber-optic systems use some type of weighted distribution calculation to smooth the spatial distribution of temperature and strain phenomena to a small interval about the sampling point. Consequently, air-water contacts and sharp changes in environmental conditions can cause abnormal behavior over a small range of positions. Selker et al. (2006) used a Gaussian distribution that scattered light wavelengths fall into to determine the statistical center of a shift caused by environmental changes. Sensor positions in the calibration bath were determined graphically; edge effects were removed by truncating up to 1.0 m of data (10 sampling points) from the ends of the defined sensor area, as shown in Figure 3.

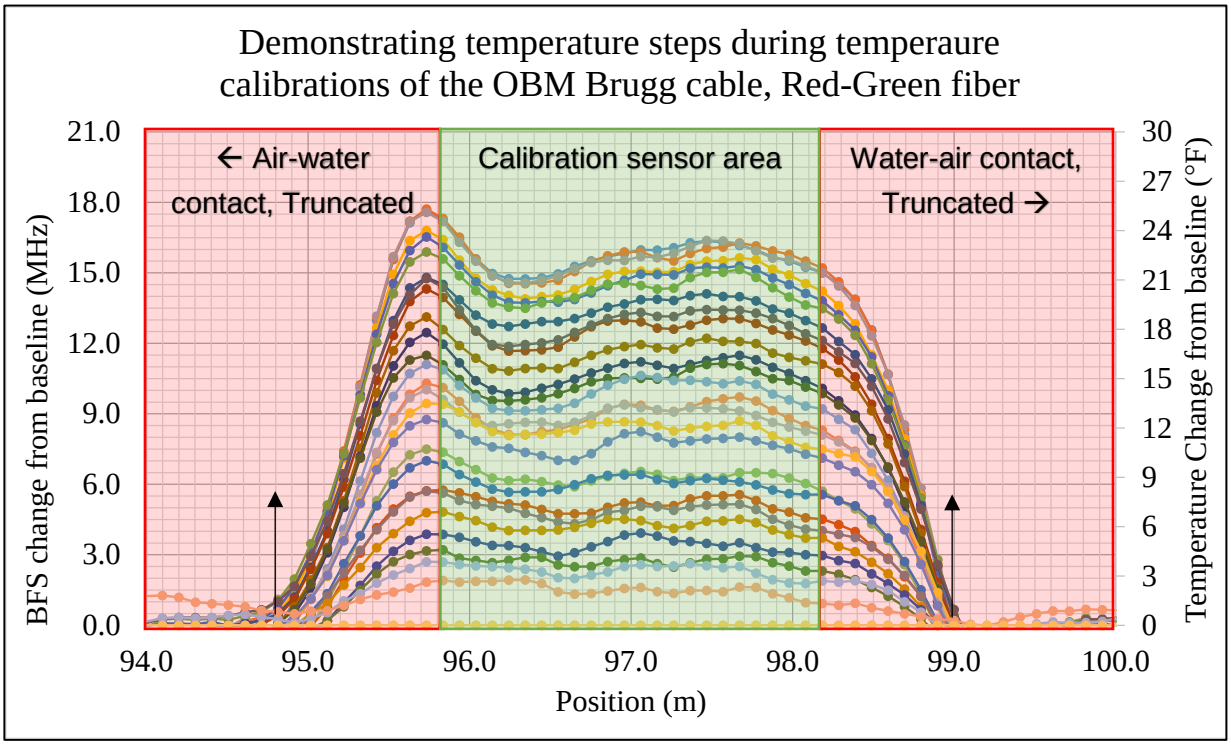

Figure 3: Scans at 10-minute intervals are represented by different colors, increasing in temperature as time progresses; tracking each sensor position through time made temperature-BFS correlations possible. Sensor truncation was necessary to isolate the calibration cable coil for the temperature-frequency response analysis. The arrows indicate the positions where the air-water transition does not influence measurements due to weighted averaging of 1m, centered on each sensor position. The "ladder" of optical scans demonstrates consistent cable sensitivity to temperature changes and a maximum temperature range ±0.8°F about the scan means.

Measurements taken by the DITEST were set with the scan scheduler to run at 10-minute intervals and time-matched to corresponding TidBit measurements. DITEST auto-calibrations and scan duration variations introduced time delays into scan timestamps, limiting time matching between the TidBits and the cable measurements to within 2.5-minutes of each other.

The heating element guaranteed temperature accuracies of ±1°F from the dial setting, which was turned to the hottest setting at ~88°F to heat the bath quickly. The transient heating phase took approximately 5 ½ hours, after which the bath temperature was maintained at equilibrium for another 6 hours. Calibrations used the transient phase to derive the sensor response to temperature changes and the equilibrium phase to examine cable responses to small changes in temperature (due to heating-element induced hysteresis).

Derive sensor frequency-measurement variable characteristics.

Linear regressions in Microsoft Excel calculated sensor response coefficients, using BFS as the dependent variable and TidBit-measured temperatures as the independent variable. The "SLOPE($Y_i : Y_n$, $X_i : X_n$)", "INTERCEPT($Y_i : Y_n$, $X_i : X_n$)", and "CORREL($Y_i : Y_n$, $X_i : X_n$)" linear regression functions in Microsoft Excel calculated the linear parameters for each sensor

position. Equations 1 and 2 represent the relationship measured BFS (Y) and temperature (X) at any point along a given sensor.

$$\boldsymbol{Y_{BFS} = mx_{temperature} + b_{intercept\ frequency}} \quad (1)$$

Equation 1 was expanded to Equation 2.

$$\boldsymbol{Y_{Measured\ BFS}\ [MHz] = m\left[\frac{MHz}{°F}\right] x_{temp}[°F] + b_{int\ freq}[MHz] + T_{correction}} \quad (2)$$

where $\boldsymbol{m}$ is the mean slope [MHz/°F], $\boldsymbol{x}$ is the measured cable environment temperature at a given position [°F], $\boldsymbol{b}$ is the intercept (baseline frequency), and $\mathbf{T_{correction}}$ is the sensor temperature bias/DITEST-induced frequency variation temperature correction value (detailed later in the "Error Minimization" section). Measured temperatures were back-calculated from measured frequencies by solving Equation 2 for $\boldsymbol{x}$, used later for residual analysis.

Linear parameters averaged across the sensor and measured for their variation demonstrated the ability of each fiber-optic cable to sense changes in temperature. A linear parameter set was generated for each sensor position, after which the mean slope, intercept value, and linear correlation coefficient were determined. Table II shows the table format used for sorting calibration data.

Table II: Calibration data organization

Example of temperature data analysis								
Date & Time	Position (m)							Water Temp (°F)
	95.937	96.039	96.141	96.243	96.345	96.447		
10/8/2015 16:59	10.714	10.713	10.713	10.712	10.712	10.712		88.763
10/8/2015 16:49	10.714	10.713	10.713	10.713	10.713	10.713		88.167
10/8/2015 16:38	10.714	10.713	10.713	10.712	10.712	10.712		87.436
10/8/2015 16:27	10.713	10.712	10.712	10.712	10.712	10.712		86.346
10/8/2015 16:17	10.712	10.712	10.711	10.711	10.711	10.711		85.577
10/8/2015 16:06	10.711	10.711	10.710	10.710	10.710	10.710		84.812
10/8/2015 15:56	10.711	10.710	10.710	10.710	10.710	10.710		84.049
(etc.)								
								Average Relationship Coefficients
Slope (MHz/°F)	0.758	0.733	0.717	0.711	0.709	0.709		0.716
Correlation R-squared value	0.998	0.998	0.998	0.998	0.998	0.997	-->	0.998

Response coefficients demonstrated a high degree of linearity with correlation "R-squared" (R^2) coefficients above 0.950 between observed BFS and gradational temperature increases. Positions within the sensor area examined for graphically apparent outliers; outliers had slope or R^2 correlation coefficient values that fell more than 5% outside of the mean value for each parameter. Deviations of slope values derived during calibration data analysis, shown as the spread of frequencies at each temperature in Figure 4, were used to calculate temperature uncertainties based on Equation 3.

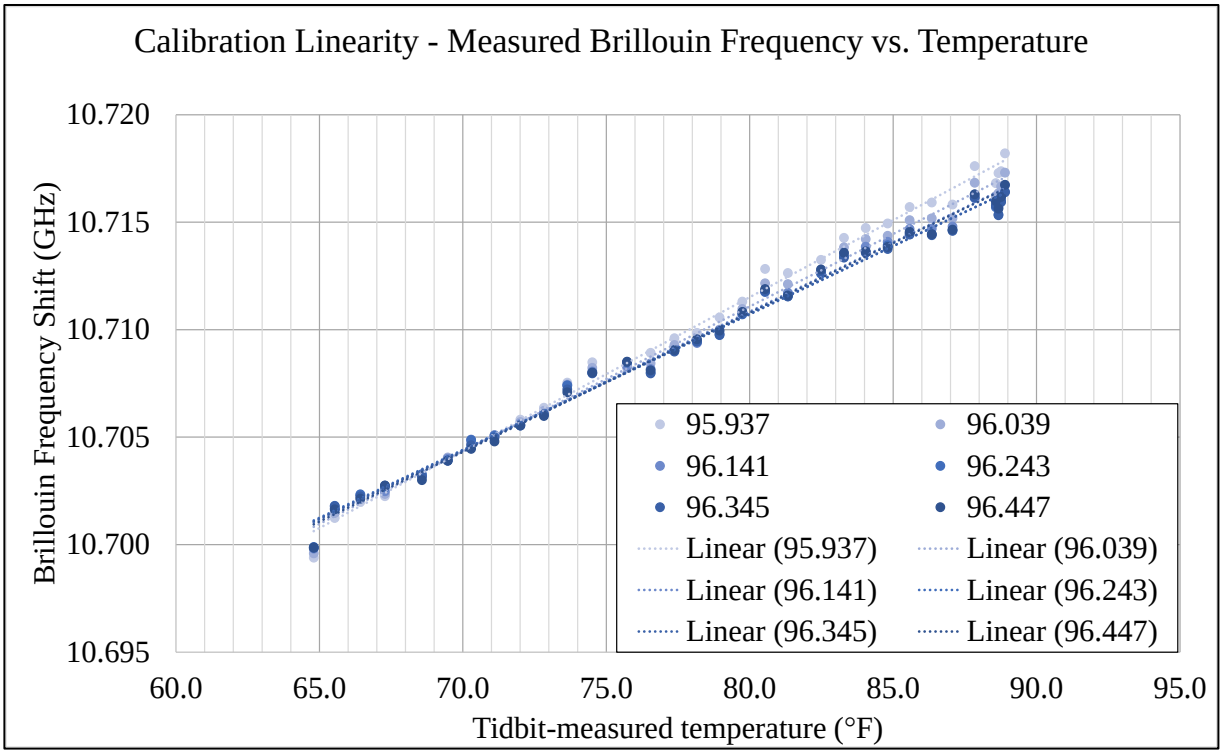

Figure 4: Variations in linear parameters, shown here as a result of slight differences in frequency responses to temperature changes at each position, were accounted for by taking the average of all parameters in the calibrated sensor, reducing error overall. The table view of the practice is shown at the bottom of Table II.

$$\frac{\mathbf{1}\boldsymbol{MHz}}{(\boldsymbol{m} \pm \boldsymbol{\sigma})} = \boldsymbol{Temperature\ uncertainty\ due\ to\ slope\ error}, \boldsymbol{^\circ F} \quad (3)$$

where sigma ($\boldsymbol{\sigma}$) is the standard deviation of the slope, calculated by the "STDEV.P($X_i : X_n$)" function in Microsoft Excel. All sensors demonstrated consistent slope values, with a maximum standard deviation in calculated values representing ± 0.05°F. Figure 5 shows the TidBit measured temperatures and the associated BFSs from all sensor positions as a scatter plot.

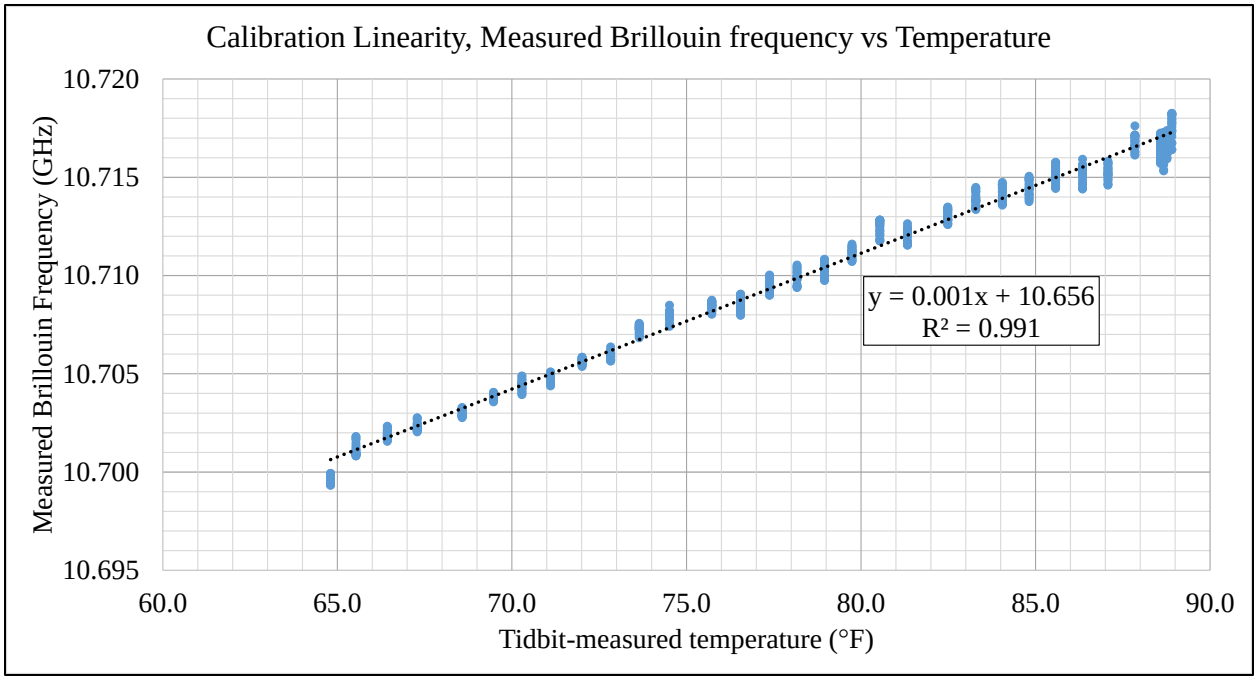

Figure 5: A line of best fit through a scatter of all the calibration data for a single sensor. Standard deviation analysis for the slope parameter (detailed by Equation 3) characterized variation about the line of best fit.

The average of each parameter for the calibrated sensor sections agreed with the generated line of best-fit when the data from all calibrated positions were plotted as one series. Linear parameters for each calibrated sensor are summarized in Table III.

Table III: fiber-optic sensor calibration summary

UMEC Fiber-optic Calibration Summary							
Physical Cable Parameters					Calibration Parameters		
Cable Manufacturer	Splice Configuration	Fiber Set	Cable length	Calibration points/length	Slope [MHz/°F]		Mean R^2 value
					Mean	Stdev	
Brugg T-85	In-house Turnaround	Red-Green	100m	23pts / 2.3m	0.691	0.028	0.997
		Blue-yellow			0.713	0.011	0.998
	Factory Turnaround	1-2	494m	23pts / 2.3m	1.037	0.016	0.997
		3-4			1.060	0.037	0.999
	Looped	Red	134m	9pts / 3.6m (0.4m resolution)	1.009	0.036	0.999
		Green			0.998	0.051	0.999
		Blue			0.978	0.025	0.997
		Yellow			1.008	0.007	0.998
Corning FREEDM-LST	Looped	Blue	250m	Not Calibrated (termination damaged during original			
		Orange		39pts / 3.9m	0.660	0.007	0.998
	Looped	Blue	200m	35pts / 3.5m	0.664	0.007	0.998
		Orange			0.661	0.005	0.998
	Looped	Blue	230m	42pts / 4.2m	0.676	0.019	0.998
		Orange			0.676	0.017	0.998

After all temperature sensors were calibrated, the project focus shifted to preparing for and executing a sensor deployment in the Orphan Boy Mineshaft.

Data Retrieval Program

Data exported from the DITEST Configurator window required direct interaction with the DITEST machine. A remote access program implemented in February 2016 eliminated the need for manual interactions to retrieve data, access permissions, and kept the DITEST from going into automated standby mode (a functionality which could not be overridden).

A free software package (TeamViewer11) obtained through the remote-access company TeamViewer allowed remote manipulation of the DITEST through any wireless network. TeamViewer 11 permits access to the DITEST except during an automated standby/reboot sequence (which takes approximately 10 minutes). Similar to moving the mouse on a computer to prevent automated shutdown, remote access allowed the re-initialization of scans or the scheduler on the DITEST. After installation, the software package was tested for its speed to determine the time between initializing the software and having full control of the DITEST; logging on from a computer terminal took about 60-seconds and logging in from a cell phone (with a good or excellent network internet connection) took about 90-seconds. Figure 6 shows an example of the TeamViewer 11 device pairing window.

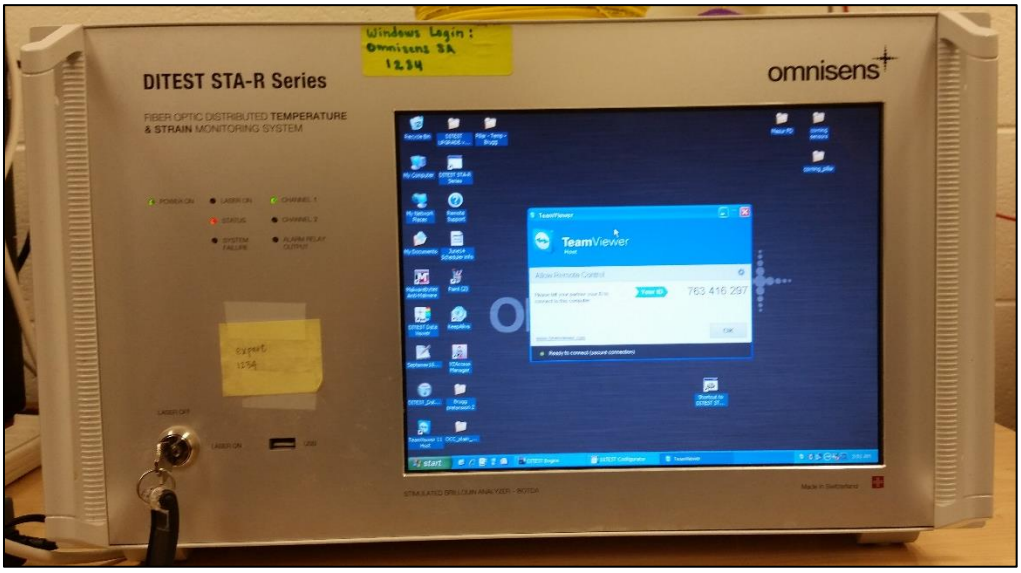

Figure 6: The TeamViewer 11 remote access program used an address key and password system, where the address key would link computer terminals and the password (set by the user) would grant full remote-accessibility. The program allowed the easy transfer of data between computer terminals similar to copying items from one folder to another on the same terminal.

One of the most useful functions of TeamViewer 11 is able to copy-and-paste data folders directly from the DITEST onto the lab computer desktop without any additional actions required. Data were uploaded to an independent Google Drive cloud archive (MTechFOSProject@gmail.com) after transferring a copy of the data to the lab computer to keep a continuous backup of all recorded data. Similarly, completed data analysis documents were uploaded to the archive and updated periodically. While other archival procedures were tested, uploading to a cloud drive prevented the unnecessary cloning of data or data analysis documents.

Using the DITEST scheduler with multiple attached sensors required the initialization of the scheduler every day at the same time to synchronize scan times between days; the scheduler would conduct automated scans at user-defined intervals for a period of up to 24-hours. Logins were scheduled daily at 11:50am, restarting the scan scheduler at 11:57am. The start time for the scheduler was adjusted with the time following the final scan in the sensor sequence, the "scan trailing time," until the last scan terminated at approximately 12:00pm each day, ±120-seconds. Figure 7 shows the scheduler window layout on the DITEST.

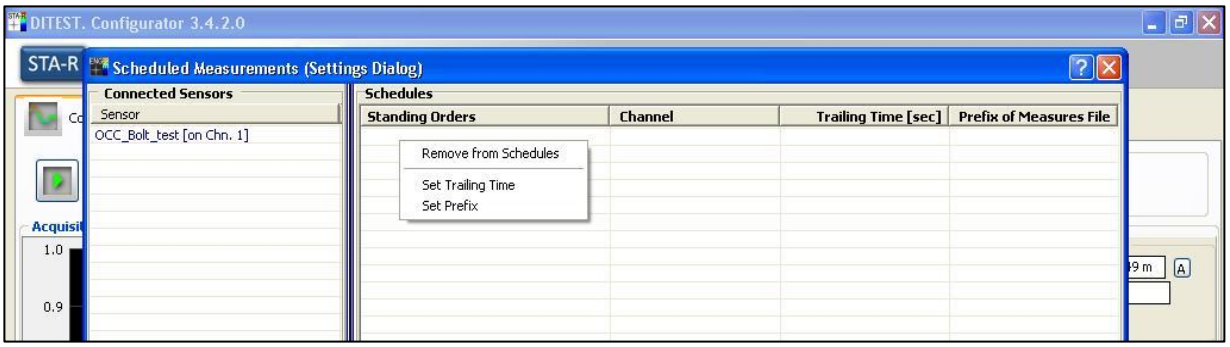

Figure 7: The user organized sensors into the desired scan order and interval using the DITEST Scheduler. Scans were then set to run with various time-delay settings in order to begin or end the sequence at a particular time. The scheduler allowed intervals between scans of up to one full day, though this is not recommended due to the automatic shutdown functionality.

Termination time variations between scan sequences raised the question of whether or not the TidBits could be used because of their advertised 5-minute equilibration time in water—a failure to equilibrate at an even rate would render the TidBits useless in a transient-phase calibration setup. This issue was later addressed using equilibration experiments.

TidBit equilibration and measurement confidence

The Onset model UTBI-001 TidBit calibration employed two groups of TidBits with different dates of manufacture, referred to hereafter as Gen-1 (pre-2014) and Gen-2 (2016), to determine if any discrepancy existed between the reference instruments. The TidBits underwent the same calibration setup as the fiber-optic cable sensors, with the heating element and the tidbits positioned in the same horizontal plane and all tidbits placed in the bath at the same time. When comparing the unprocessed temperatures, the maximum temperature difference between any two TidBits was 0.13°F and a difference between the Gen-1 and Gen-2 averages of 0.07°F. Figures 8 and 9 show both groups within the advertised accuracy bound of ±0.36°F (±0.2°C).

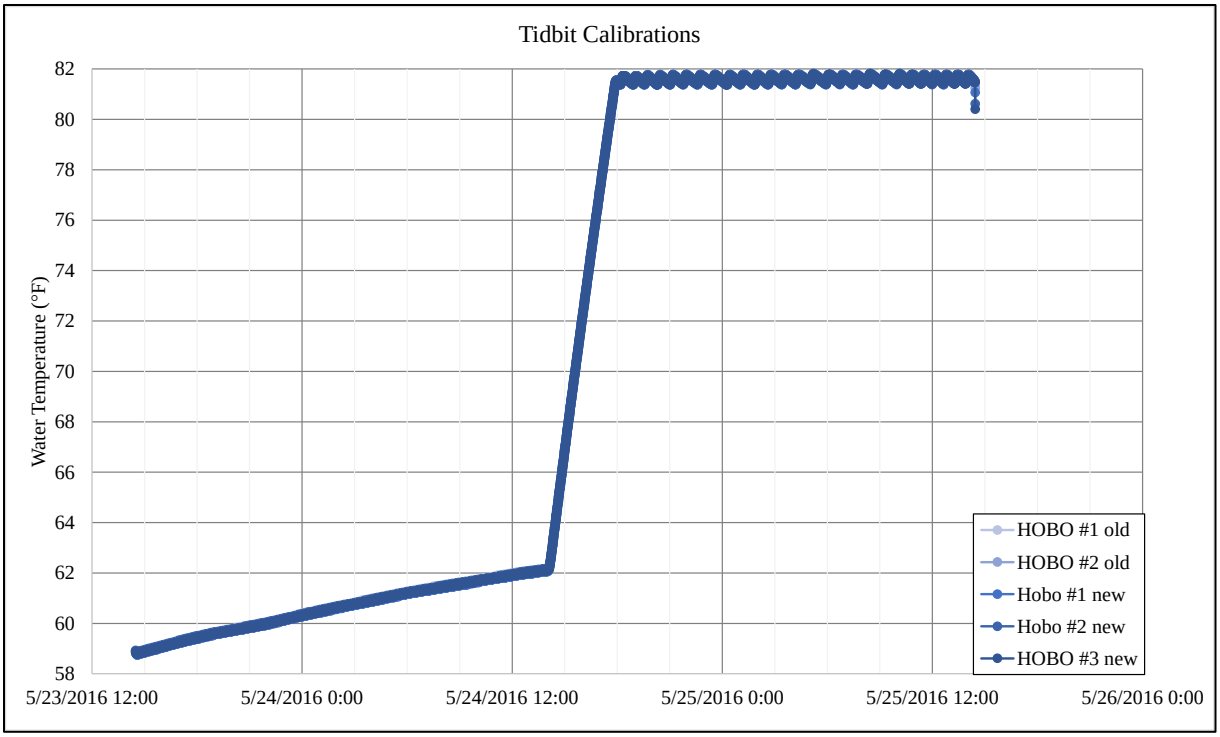

Figure 8: As demonstrated by the graph above, the measurements of the different generations of TidBits were very close. Calculations rendered a maximum difference of approximately 0.1°F.

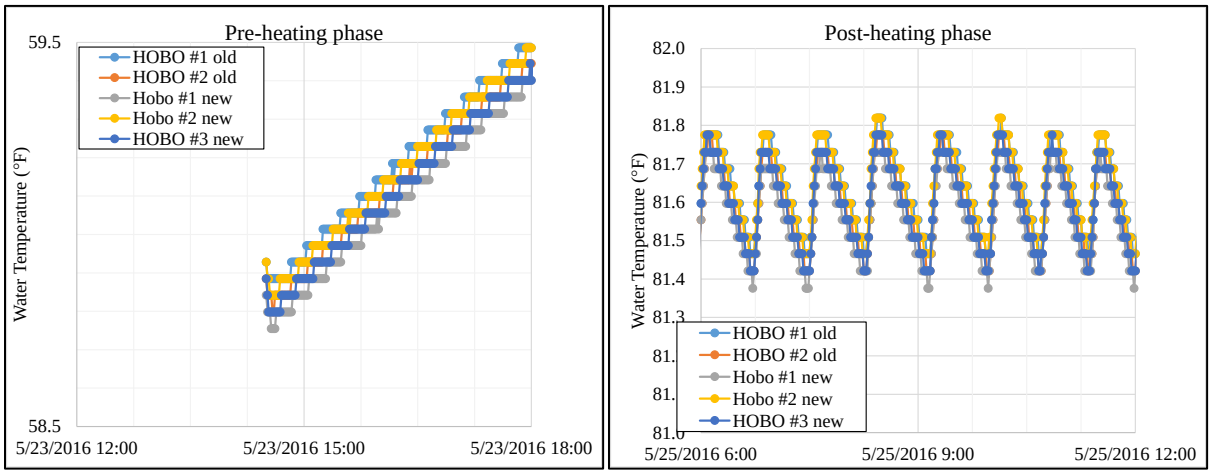

Figure 9: Views of the temperature measurement differences between the two groups of tidbits (left) in cold tap water as the bath warmed to room temperature and (right) at the high-temperature equilibrium, set to 82°F. The heater tolerance reported by the manufacturer was ± 1°F. Temperature variations were minimal, as mentioned on the previous page.

Instrument equilibrium can be described in a couple different ways. First is by establishing a theoretical rate of change, for example, the temperatures measured at two different times, then determining the rate of variable change detected at different time intervals; the time-interval that detects the value closest to the theoretical value is considered the time required for equilibration. This may result in hysteresis, where the detection of changes in the value of a

physical property like temperature lag behind the actual change, causing an abnormally high measurement. Of course, accepting the manufacturer-advertised equilibration time in the media as fact requires no additional work. Equations 4 and 5 describe the difference between consecutive temperature measurements,

$$\Delta \boldsymbol{T_i} = (\boldsymbol{T_{n+\Delta t}} - \boldsymbol{T_n}) \tag{4}$$

$$\boldsymbol{Error} = \frac{(\Delta \boldsymbol{T_i} - \Delta \boldsymbol{T_r})}{\Delta \boldsymbol{T_r}} \tag{5}$$

where ΔT_i represented the difference between consecutive measurements, T_n and $T_{n+\Delta t}$, separated by the time interval Δt. The average temperature difference was approximately 0.086°F using a time interval of 1-minute. Tabulated temperature difference data showed 83% of all measurement values were 0.086°F, suggesting 95.6% of the full value could be reached with an interval of 1-minute and a full-value measurement obtained between 1-2 minutes. At 0.086°F, the error present in ΔT_i was ~4.4%. Figure 10 shows the hysteresis caused by the short duration of the measurement interval.

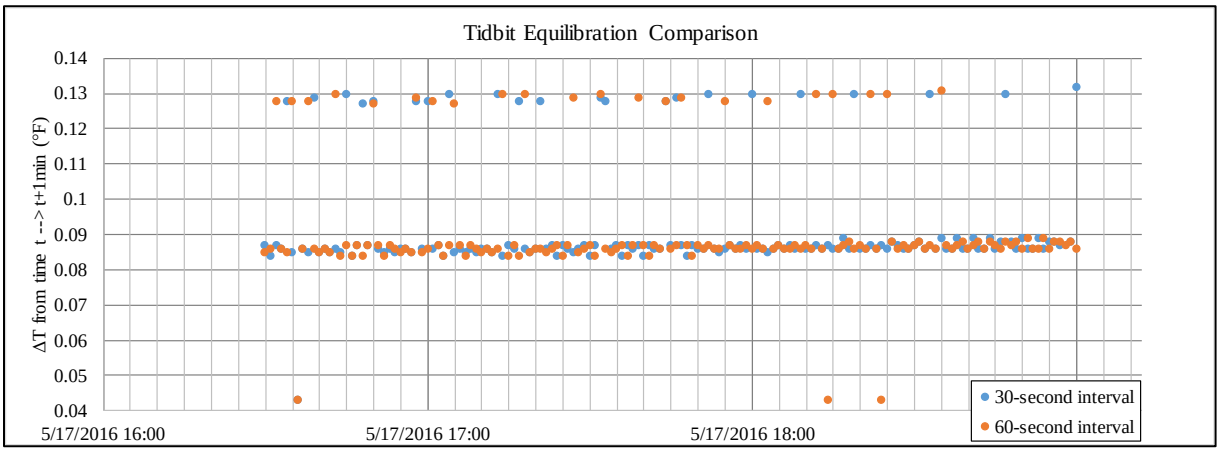

Figure 10: Measurement confidence and hysteresis went hand-in-hand in this experiment, with 83% confidence reached with a 60-second measurement interval; other data points were evidence that hysteresis was still present using this measurement interval.

Thomas Coleman is a consultant from Silixa Ltd., fiber-optic sensor company; Mr. Coleman overruled the need for fiber-optic equilibration-time experiments because sensor cables are designed to equilibrate within seconds of experiencing environmental changes in all mediums. Equilibration experiments could not be performed without having a master-technician level knowledge of the DITEST software and hardware. Based on Mr. Coleman's statement suggesting fiber-optic equilibration times less than 10-seconds, and the problem of limited technical knowledge of the DITEST, Mr. Coleman's advice was followed and equilibration experiments were not conducted on any cable sensors. After confirming the TidBit measurements from the calibrations were valid (the measurement interval was 5 minutes, well within equilibration time), the next step was to examine and correct for residual errors.

Error minimization: Fiber-optic measurements vs. TidBit measurements

Minimizing calibration calculation errors helped to define an expected error present in calibration data collection and analysis. To accomplish this, the derived relationship coefficients were used to back-calculate temperatures measured by the fiber-optic sensors during the calibration scans. Figure 11 shows a plot of the back-calculated temperature profiles, measured relative to the first scan in the calibration sequence.

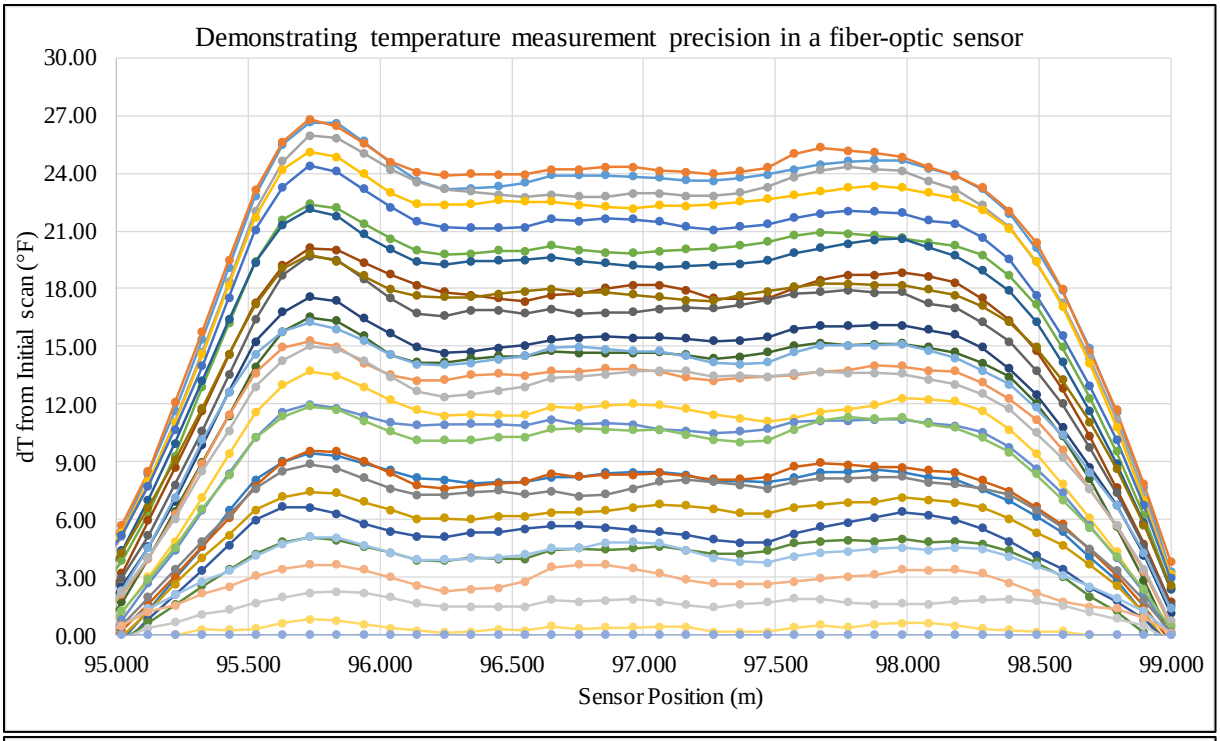

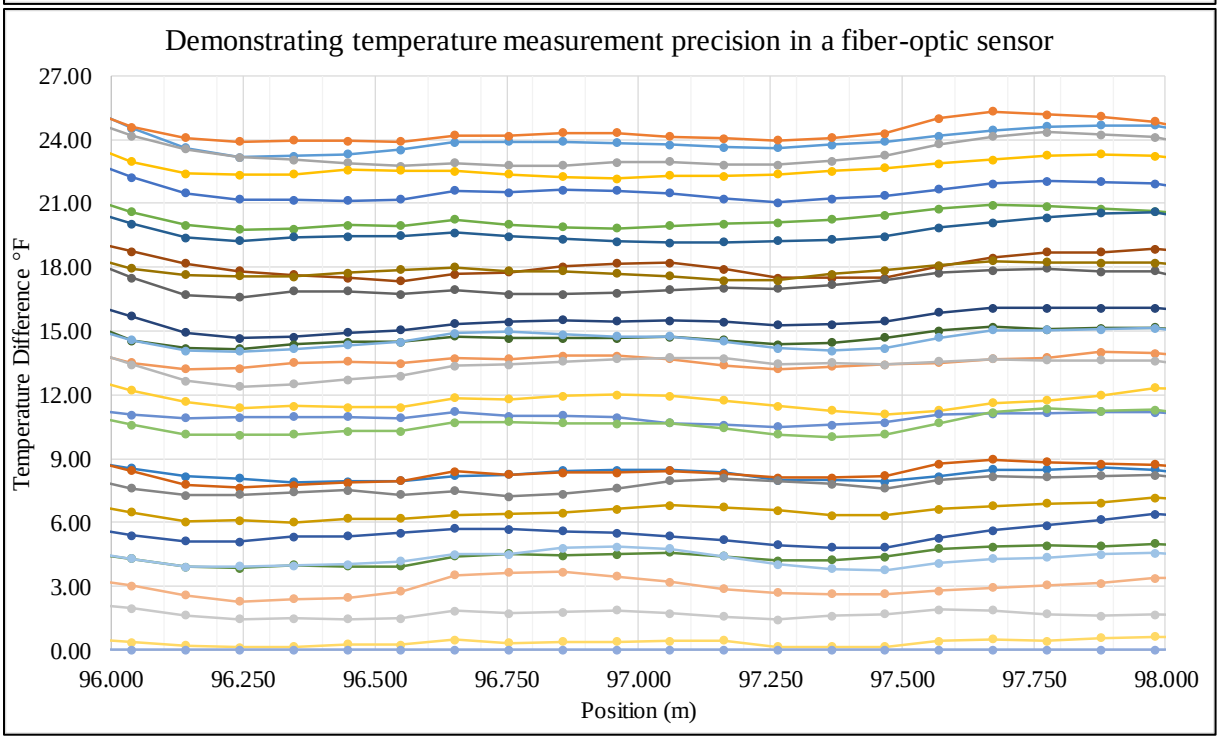

Figure 11: Back-calculated temperatures showed little variation over the length of the calibrated sensor length. After sensor truncation to account for edge effects, the temperature profile (top) was transformed into a temperature ladder (bottom); fiber-optic measurements showed variation of about ±0.4°F about the mean for each "rung" of the ladder.

The initial calibration scan was removed to eliminate frequency variations (and thus temperature variations) from manufacturing-induced refractive index dissimilarities between sampling points.

The error minimization process began with subtracting the tidbit-measured temperature from the optical ones to create a set of residuals. Hurtig et al. (1996), Hauser et al. (2013), and Aminossadati et al. (2010) indicate potential accuracies of Raman-based optical sensors of ± 0.54°F, ± 0.68°F, and ± 1.8°F respectively [resolution capabilities are system specific]. These accuracies consider the mean bias (temperature offset) of cable sensor measurements to the reference and indicate the need for correction prior to analysis. The RMSE was calculated using Equation 6,

$$\boldsymbol{RMSE} = \sqrt{\frac{\mathbf{1}}{\boldsymbol{n}}\sum_{\boldsymbol{i=1}}^{\boldsymbol{n}}(\boldsymbol{T_{i\ measured} - T_{i\ expected}})^{\mathbf{2}}} \tag{6}$$

where $\boldsymbol{n}$ is the number of measurements taken, $T_{i\ measured}$ was the cable-measured temperature at time $\boldsymbol{i}$, $T_{i\ expected}$ was the TidBit-measured temperature (this could also be viewed as "measured"-"reference"), and the summation notation represents the average of the squared residuals. Figure 12 shows a sample plot of the residuals and the potential range of variation.

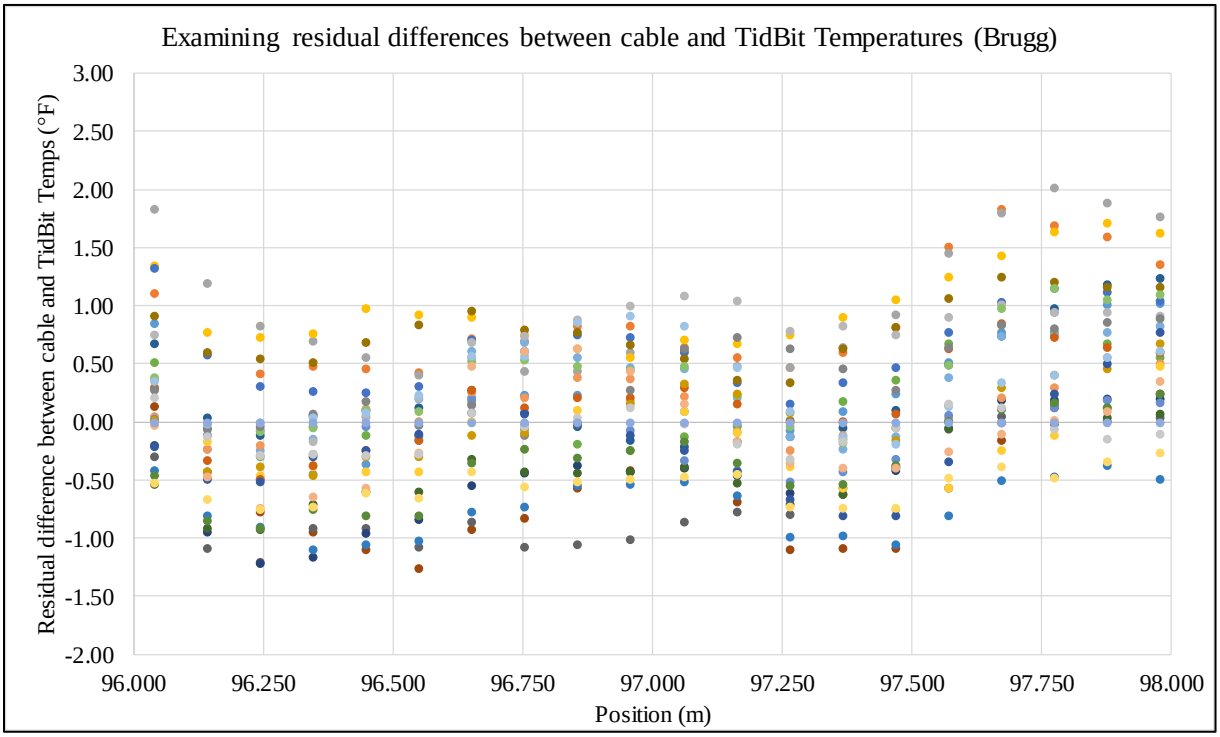

Figure 12: Temperature offsets between Brugg T-85 and TidBit-measurements on either side of the bulkhead termination; statistical analysis suggests an average RMSE of 1.54°F and 1.41°F, respectively.

Sinusoidal swings in temperature are likely a factor of the cable geometry in the calibration bath, where some parts of the cable coil are farther from the heating element than

others. Table IV shows an example of the format for calculating the RMSE for the temperatures measured at each position.

Table IV: RMSE calculation practice

ith measurement	Cable temperature $T_{i,\,measured}$	→	Tidbit Temperature $T_{i,\,ref}$	→	Temperature Residuals	→	Squared Residuals	→	RMSE for one sensor position	
10/8/2015 16:58	24.7		23.661		1.047		1.097		RMSE	1.53
10/8/2015 16:47	25.0		23.477		1.477		2.183			
10/8/2015 16:37	22.6		22.334		0.247		0.061			
10/8/2015 16:26	22.6	-	21.607	=	0.959	$(T_{i,\,measured} - T_{i,\,expected})^2$	0.920	(Equation 6)		
10/8/2015 16:15	22.4		20.882		1.554		2.414			
10/8/2015 16:05	21.4		20.070		1.309		1.714			
10/8/2015 15:54	21.2		19.350		1.812		3.283			

RMSE correction values were determined by subtracting a small (1.0ºF) test value from the cable-measured temperature, then iterating in 0.01ºF steps and recording the change in the mean RMSE until minimum value was achieved. Figure 13 shows a sample of the temperature correction optimization.

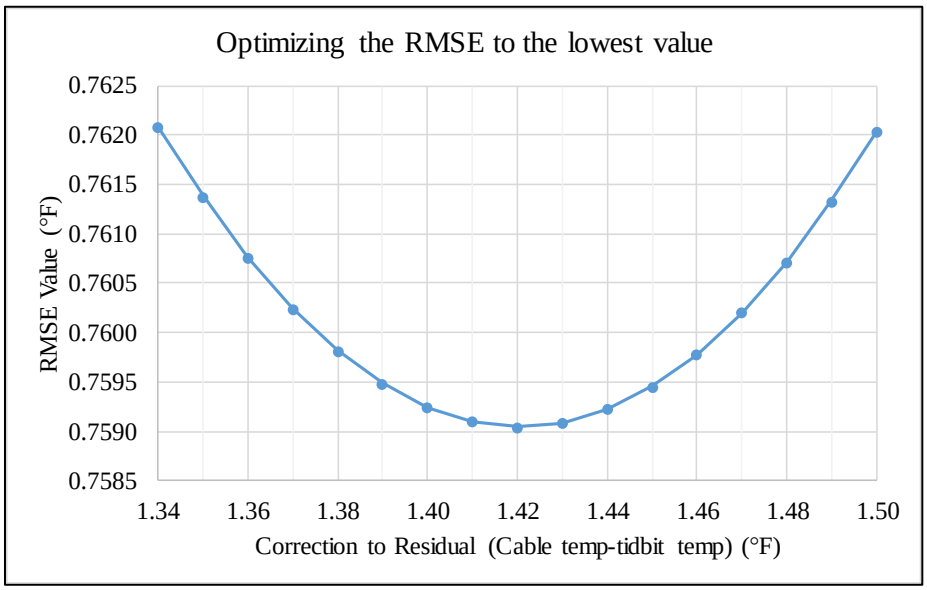

Figure 13: RMSE-minimizing temperature correction values were selected from the iterative optimization process.

Residuals were reduced to a minimum RMSE of ± 0.76°F after subtracting the optimized correction value from the measured cable temperature, reported here as the accuracy of the respective cable sensors following the practice by Hausner et al. (2013). RMSE values calculated for both the transient and equilibrium heating phases demonstrated similar RMSE values, about 1.0-1.5°F before correction. The RMSE values calculated from the transient phase were used to represent the calibrated sensor. While residual values varied, the residuals were distributed evenly about the 0°F line for all but a few sensors. Therefore, single-parameter corrections were applied to all sensor positions with confidence. Calibration correction parameters are compiled in Table V.

Table V: Error Minimization Summary

Calculated RMSE Values											
Cable Manufacturer	Splice Configuration	Temperature Variation [°F] for frequency uncertainty [MHz]			Uncorrected RMSE	RMSE STDEV	Corrected RMSE	Corrected RMSE STDEV	RMSE Correction (Residuals - cor.)	Uncorrected Mean Sensor Bias (°F)	Corrected Mean Sensor Bias (°F) using RMSE correction value
		0.70MHz	0.85MHz	1.00MHz							
Brugg T-85	In-house Turnaround	1.0	1.2	1.4	1.5	0.5	0.8	0.2	1.4	1.4	0.0
		1.0	1.2	1.4	1.4	0.2	0.8	0.0	1.2	1.2	0.0
	Factory Turnaround	0.7	0.8	1.0	0.6	0.1	0.6	0.1	-0.1	-0.1	0.0
		0.7	0.8	0.9	0.7	0.3	0.5	0.2	0.5	0.5	0.0
	Looped	0.7	0.8	1.0	RMSE Analysis incomplete						
		0.7	0.9	1.0							
		0.7	0.9	1.0							
		0.7	0.8	1.0							
Corning FREEDM-LST	Looped										
		1.1	1.3	1.5							
	Looped	1.1	1.3	1.5	0.6	0.1	0.6	0.0	0.2	0.2	0.0
		1.1	1.3	1.5	1.3	0.4	0.7	0.1	1.1	1.1	0.0
	Looped	1.0	1.3	1.5	0.6	0.2	0.6	0.2	0.2	0.2	0.0
		1.0	1.3	1.5	0.9	0.3	0.7	0.2	0.5	0.5	0.0

Using the RMSE, the application of a fixed temperature correction according to each sensor type is reasonable and places the accuracy of our system at the maximum corrected RMSE, ±0.8°F.

Measurement variability due to DITEST operation

A repeatability experiment utilized repeated scans on a sensor to reveal measurement variations between DITEST-1 (manufactured in 2009) and DITEST-2 (manufactured in 2013) (identical in software). Ten scans generated data characterizing the variability induced by the DITESTs during repeated measurements at equilibrium. Using a sensor spatial resolution of 0.1m, 504 data points (5.0m sensor) were examined using DITEST-1 and 685 points (6.8m sensor) were examined using DITEST-2. The standard deviation was calculated at each sensor position using the ten scans, after which they were plotted in histograms to create distribution plots for graphical analysis. The mode values of the distributions were DITEST-1: 0.8-0.9MHz and DITEST-2: 0.7-0.8MHz, indicating significant measurement instability using rapid scanning and fine spatial resolution selections.

Calibration errors were addressed, allowing the project to proceed to monitoring in the OBM.

Temperature profiles & Time series analysis

The term “temperature profile” refers to the collection of temperature measurements at every sampling point on a cable sensor associated with a time-stamp for the entire collection. Temperature profiles tracked temperature changes through time according to the sensor position. Time-series analysis looks at the temperature measurements from multiple dates at a single position, plotting the history of temperature change at that position.

A cluster of cable sensors including Brugg T-85, Corning FREEDM-LST, and Brugg “legacy” cable (from early work in 2014, similar in design to T-85) were deployed vertically in the OBM on 12-December-2015. The cluster was positioned to monitor the portion of the shaft below the access point adjacent to the power room, providing vertical spatial resolutions of 0.1m, measuring temperatures for the approximately 82m (~270ft) of instrumented shaft. The cluster of sensors was attached to a PVC pipe and fed to depth, ensuring full depth was reached without obstruction. Scans have been run hourly, optimized for temporal data resolutions and remote access timing. Monitoring during the 25-February-2016 to 28-July-2016 period employed remote

access with TeamViewer to keep all systems actively scanning; data retrieval occurred twice monthly and collected data were backed up to multiple independent archives. A schematic view of the sensor deployment is shown in Figure 14.

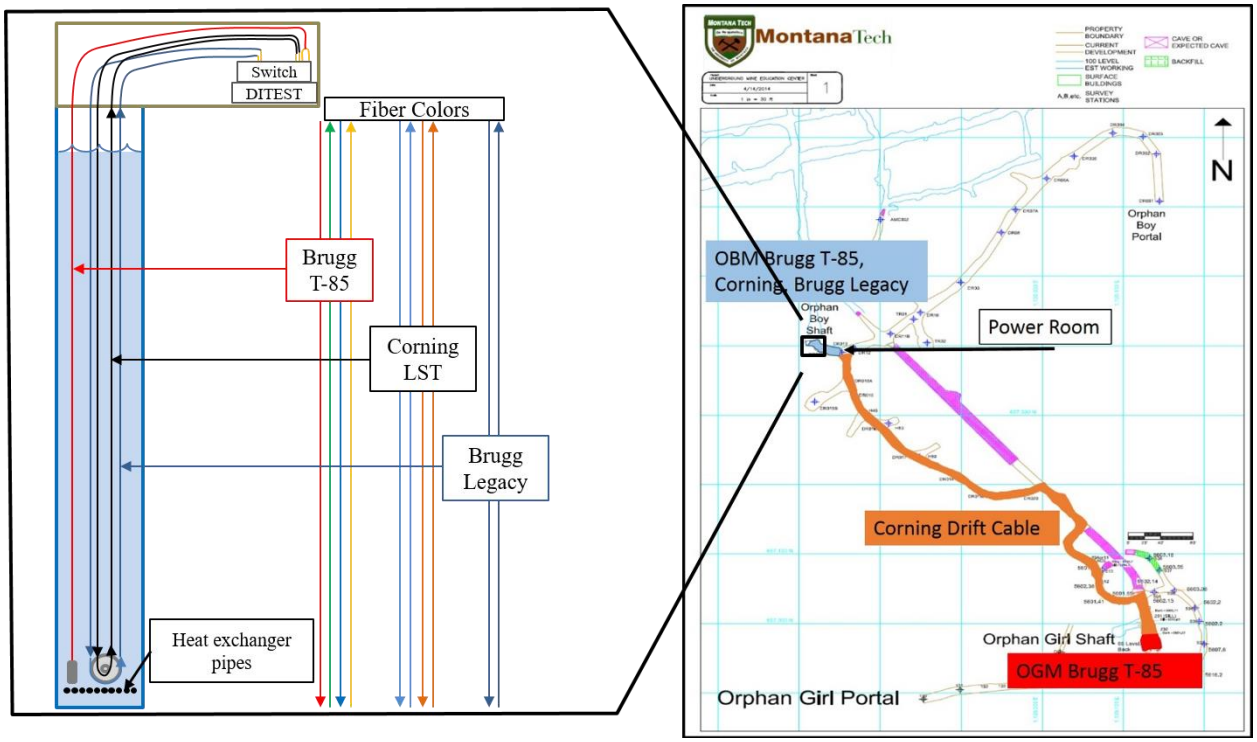

Figure 14: The cluster of fiber-optic sensors reached a depth of approximately 82m (~270ft) below the water surface, measuring water temperatures in the area above the cluster of GHES pipes at ~91m (300ft) depth. Two different looped configurations were used, one as a basic cable loop (Corning) and the other with fiber pairs spliced back on one another (Brugg T-85).

Hourly temperature monitoring began in the Orphan Boy Mineshaft on 25 February 2016. The DITEST used two sensors, one Brugg T-85 cable 94m long and one Corning FREEDM-LST cable 200m long. The Brugg Legacy cable was calibrated in a different manner during work prior to my involvement on the project, so it was recovered and deployed but was not used as a primary sensor.

Defining sensor positions in real space

Hand measurements were initially used to approximate the location of sampling points on the cable. A new method employed the use of a heat gun to identify points of interest by:

1) Scanning the sensor for a baseline profile
2) Heating a point of interest with a heat gun, being careful to keep the heat low so as to not damage the sensor
3) Stop heating and immediately scan
4) Identify the new BFS spikes caused by the heat gun by setting the initial, unheated scan as the baseline
5) Record position value and notes about the position (if used for correlating to a map)

6) Repeat as needed, moving from the sensor connection at the DITEST (so the position value is always increasing)

Location-finding experiments should be performed moving in one direction along the cable, in order to avoid any confusion relating the scan data to field notes. Heated positions identified cable positions within ±5cm of the actual heated location. Sensor position definition was essential for correlating temperature changes with the correct sensing location (and medium). Figure 15 shows a plot of particular points of interest using the above location-finding process.

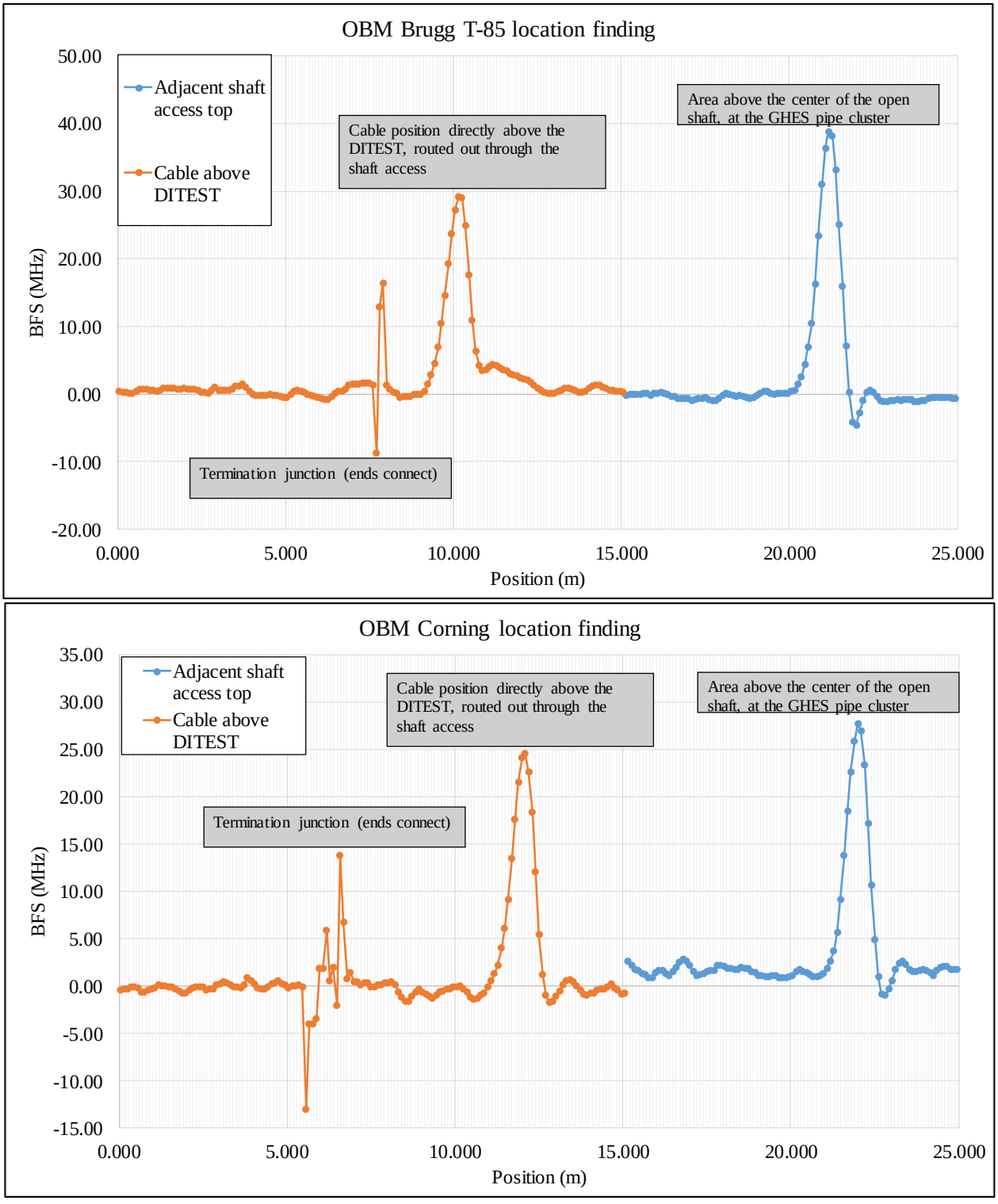

Figure 15: Location finding experiments found sensor positions on the cables directly above the DITEST and the top of the shaft access where the Geothermal Heat Exchange System (GHES) turns down into the shaft.

Water level records from the Groundwater Information Center (GWIC) managed by the Montana Bureau of Mines and Geology (MBMG) show groundwater levels at 100.0 ± 1.0ft

below ground level from January-July 2016, the most recent data available (Figure 16). A Keck Water Level Meter found the water surface position 3.50m below the top of the shaft. The position measured by the water surface locator tape combined with the distance measurement to the point above the shaft access represents the DITEST-defined water surface position within ±5cm.

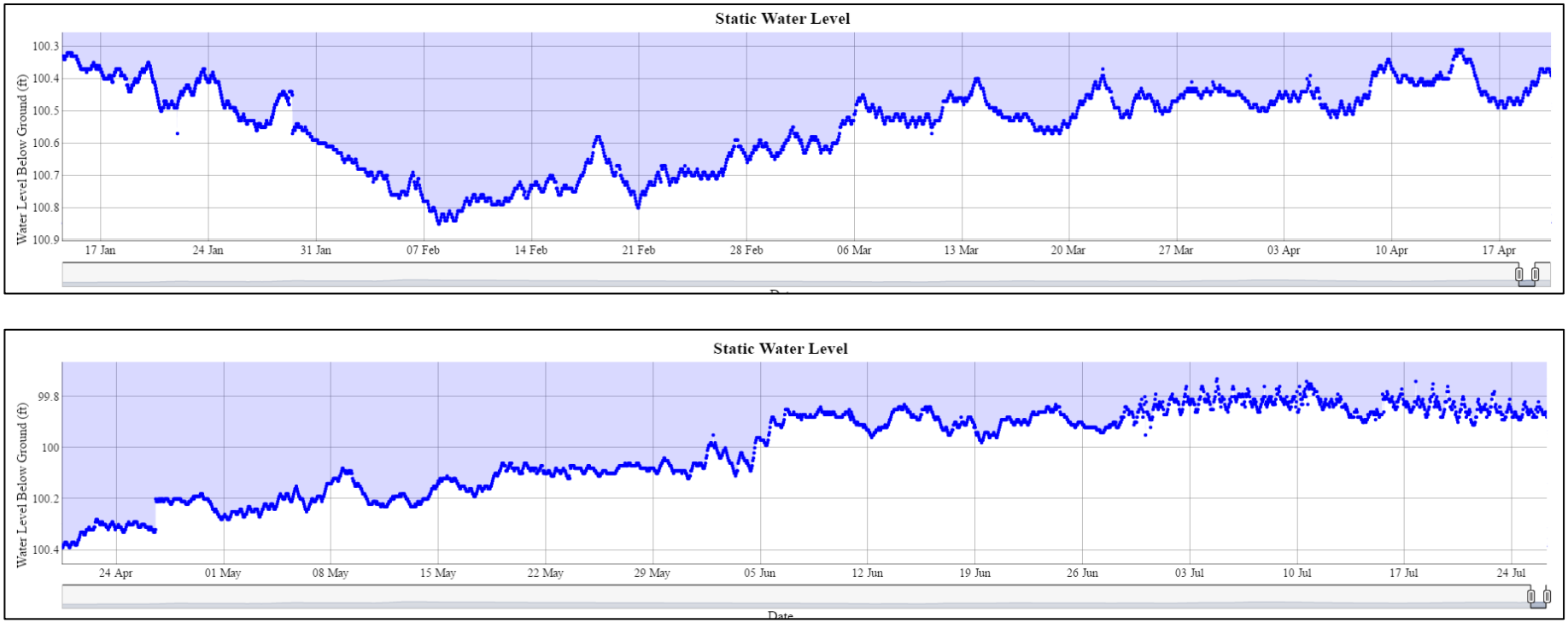

Figure 16: Water levels from the GWIC Well 4822 (which *is* the Orphan Boy Mineshaft) show very small variation about the 100ft. below ground level datum, on average about ±0.5ft.

Results

Mine water temperature vs. Time

The primary objective in the final stages of the project was capturing natural- and human-induced thermal variation in the Orphan Boy Mineshaft via deployment of a cluster of fiber-optic cable sensors. Natural sources for variation could include groundwater inflow, infiltration by meltwater, circulation by convection, and geothermal heating, among others. The operation of the GHES and use of the mine water by UMEC classes would introduce variations by withdrawing and depositing heat and shifting the water column position (thus causing shallow positions to experience large temperature shifts).

The GHES was not in operation for most of the February-August 2016 time-frame per Mack Wallace (Personal Communication, 24 Aug 2016), the consultant originally tasked with monitoring the system. A test of the GHES was performed during the May-June period per Gary Icopini (Personal Communication, 22 August 2016), which provided a significant temperature event for system assessment, checked against reference temperature data provided by Dr. Icopini and the MBMG. Figures 17, 18, and 19 show the monitoring results from the Brugg T-85 temperature sensing cable. Note, the scans shown in Figures 17-19 are temperature changes relative to the scan from 25 February 2016 at 12:00pm. Periods of experimentation with strain-sensing fiber-optic cables in August 2016 (Calvin Kammerer's portion of the project) caused data gaps during the connection of new sensors. System errors in late July corrupted data through the end of the monitoring period in August, leaving a window of viable monitoring data from February to the end of July.

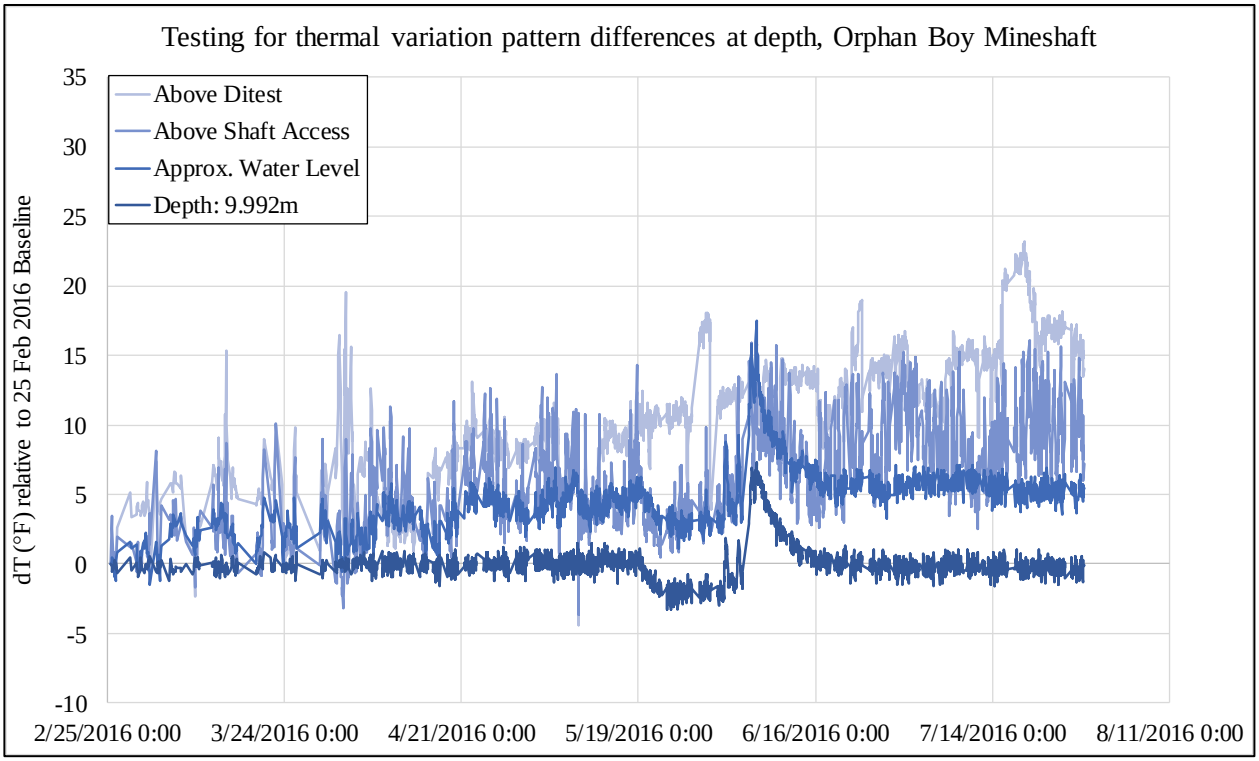

Figure 17: Temperatures above the DITEST and above the shaft access were the most variable because of the drafts that pass through the mine from the Orphan Girl side to the Orphan Boy side. Positions near the water showed similar patterning, with higher temperatures near the water surface on average.

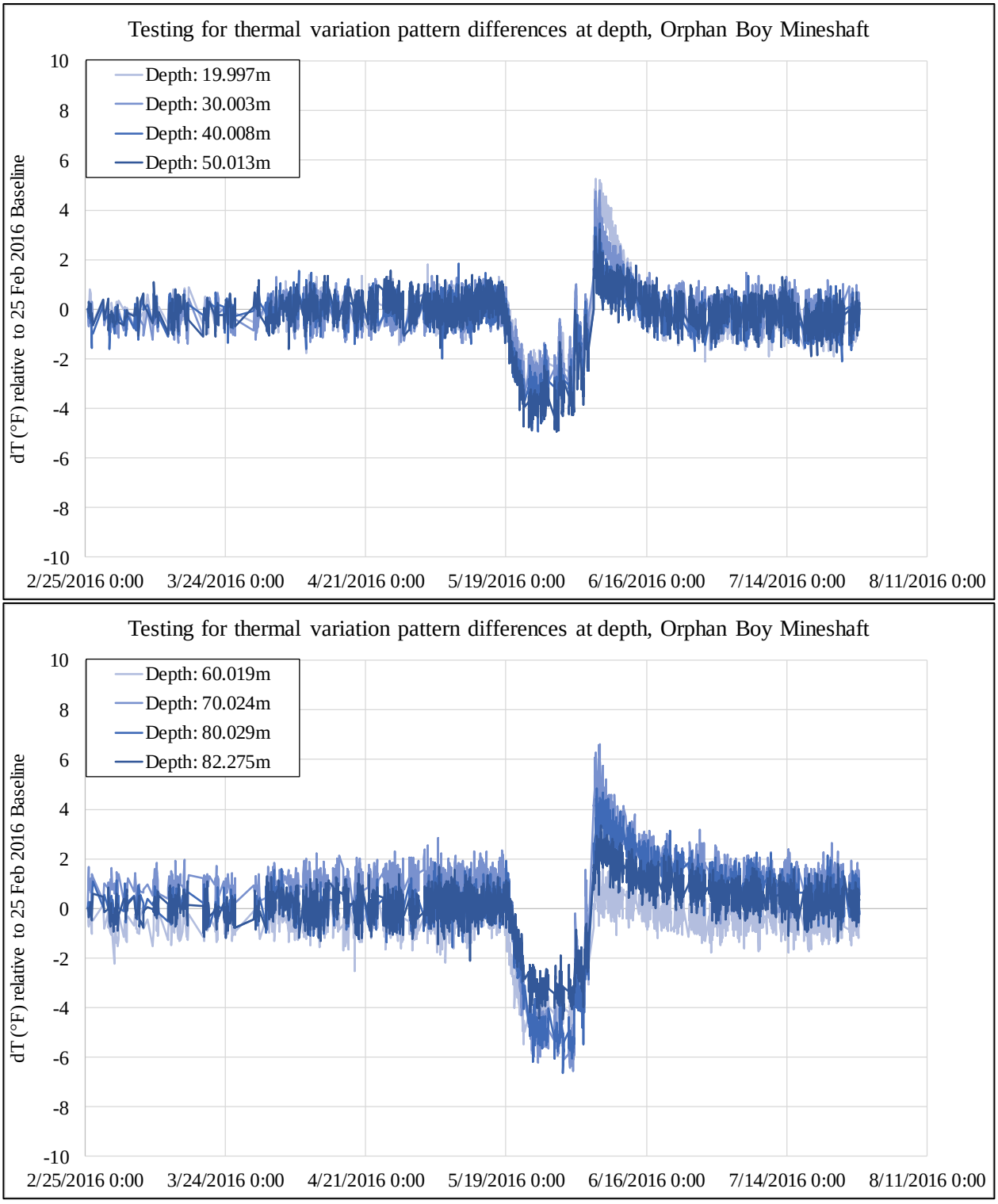

Figure 18: Submerged sensor positions showed a daily variability of approximately ±1.0ºF, with slightly increased variability of approximately ±1.5ºF during the April-May and July periods. Significant cooling period and warming event are shown during the mid-May to June period.

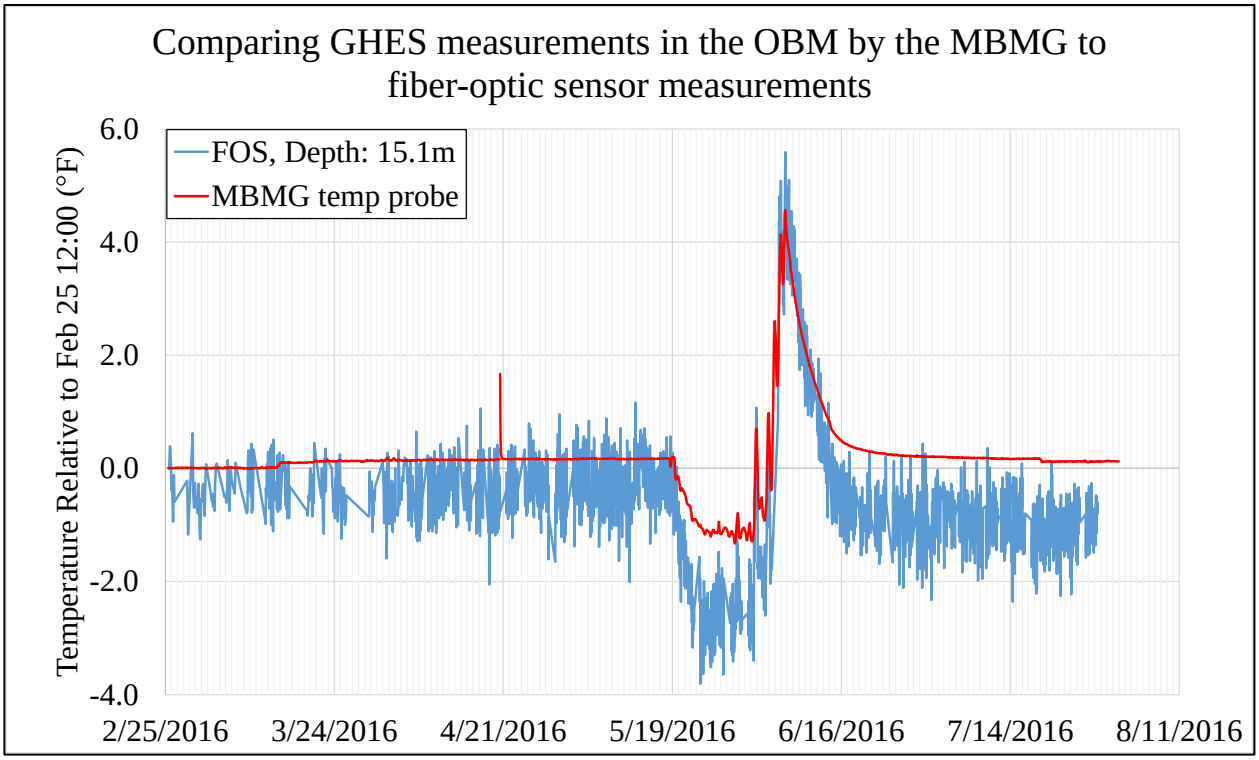

Figure 19: Fiber-optic data showed a negative bias relative to the data from the MBMG temperature probe. The profile patterns were similar, with temperature spikes at the same date and time. Fiber-optic sensors demonstrated significant variability throughout the profile; one possible explanation is the fine spatial resolution (0.1m) and its inability to smooth BFS spikes between sampling points, resulting in a highly variable profile.

Sensor positions out of the water and at the water surface showed the most variation. Submerged sensor positions showed daily fluctuations of approximately ± 2ºF, whereas sensor positions in air showed daily fluctuations of approximately ± 5ºF, with change occurring more quickly in air due to its low thermal mass. The secondary escape is located directly above the flooded shaft and allows airflow through the mine, even with the main decline gate closed on the Orphan Boy side.

Mine water temperature vs. Depth

The fiber-optic sensor cluster recorded a test of the GHES and yielded a similar temperature profile to data collected 50-feet below the static water level by the MBMG. The data provided by Gary Icopini showed a drop in temperature during the heating cycle (heat withdrawal from the shaft water), then a spike in temperature during the cooling cycle (heat deposit into the shaft water). Figure 20 shows a depth profile plotted before the test and at the temperature minimum (T-min) and maximum (T-max) during GHES operation.

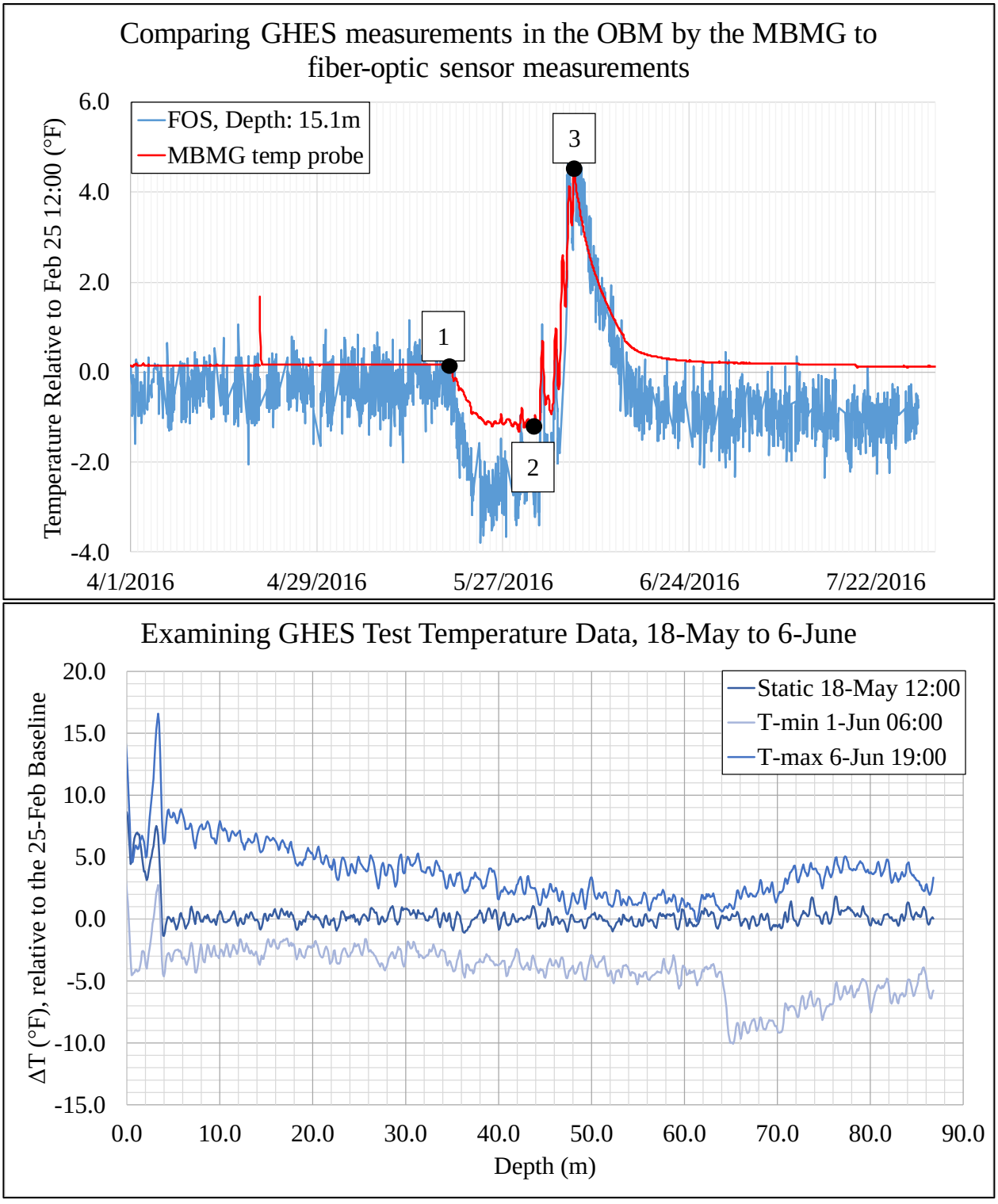

Figure 20: An examination of mine water temperatures with respect to depth showed (1) a static temperature profile at all monitored depths, (2) a negative temperature bias from the static temperature, with a sharp drop in temperatures at approximately 64m depth, and (3) a positive temperature bias above the static profile.

During periods of thermal equilibrium, water temperatures are expected to increase evenly with depth according to the thermal gradient, remaining stable at each sensor position. The static temperature profile (T-stat) measured before the GHES test showed equilibrium at all sensor positions with fluctuations of about ±1.0°F (attributable to the FOS system errors).

The T-min profile showed a negative bias of about 3.5°F below T-stat, dropping to approximately -4.5°F near 60m depth. Upon reaching 65m depth, the T-min profile shows a marked drop to approximately -10°F, increasing steadily back to -5°F from the 64m to 82m depth positions. The even temperature pattern in the upper portion of the shaft suggests water circulation 0-65m depth; the sharp drop at 65m depth is of unknown cause. The increase in temperature from 65m to 82m depth is a result of geothermal activity, as heat was being actively withdrawn by the GHES (no other heat input is immediately apparent from the data profile).

The T-max profile shows a positive bias of about 8°F near the top of the shaft. As the geothermal heating gradient is lower at shallower depths, the deposit of heat in the shaft would have a more significant impact on surface waters than those at greater depth (and thus under greater geothermal heating). The temperature difference between the working fluid in the GHES and the mineshaft would thus be greater near the surface, causing less heat to be deposited as depth increased. The temperature hump from 65m to 82m depth in the T-max profile indicates a sudden increase in the temperature difference between mine water and the GHES working fluid, supporting the data from the T-min scan which showed a sharp decrease in mine water temperature. The temperature drop near 65m depth may be a result of groundwater inflow, another level of the mine, or some other unknown source.

Measurement comparisons using identical sensor paths

After validating fiber-optic sensor sensitivity in the OBM, measurement repeatability was the next target for field experimentation. Numerical and graphical similarities between measurements entering the OBM and returning to the DITEST. Patterning was similar between the “down” and “up” portions of the sensor cluster; temperature differences between the two paths varied with a maximum difference of 2ºF. The overlapped path allowed measurement value comparisons at identical physical sensor locations.

Figures 21 and 22 show a sample of the pattern comparisons using the average of several sequential scans. Studying these discrepancies is recommended for future work.

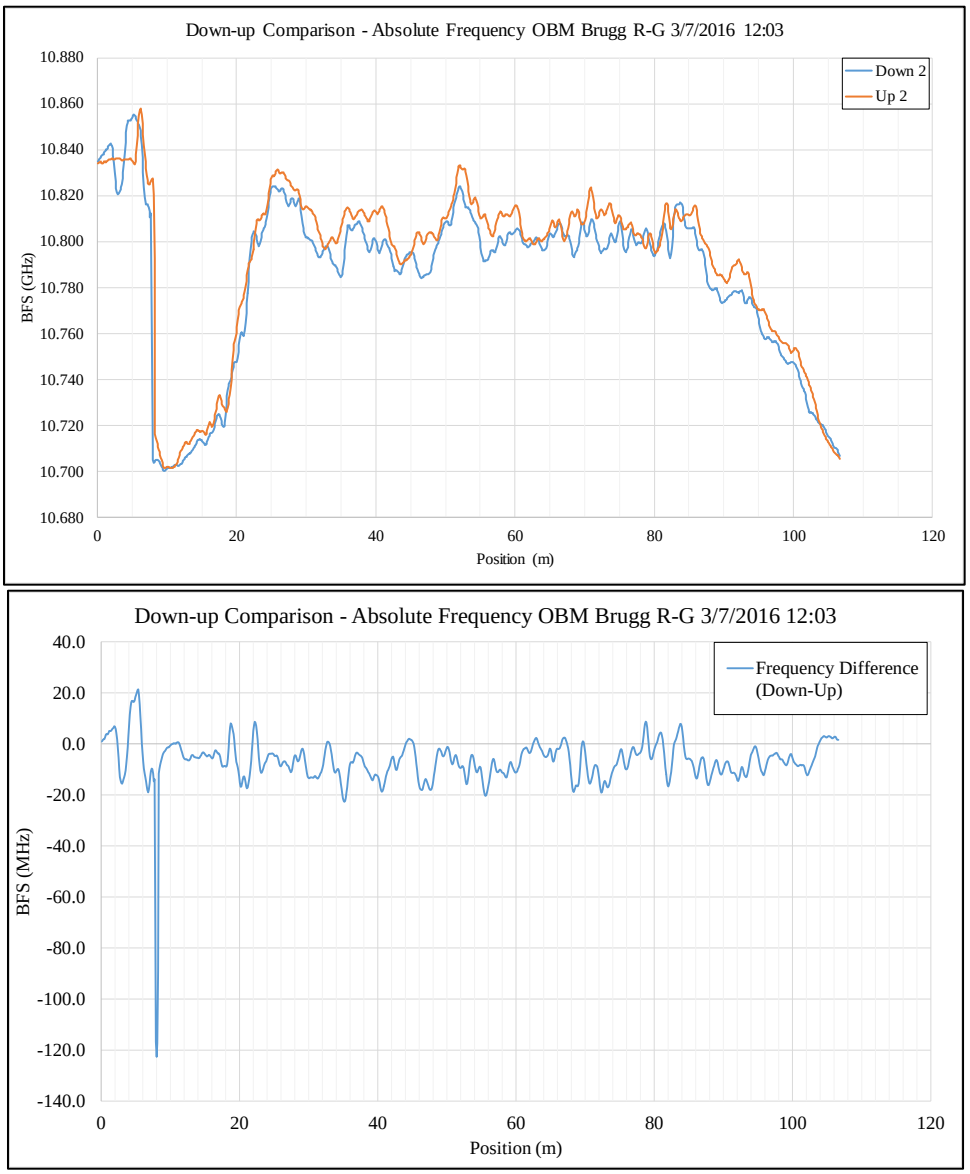

Figure 21: Brugg T-85 temperature measurements compared down and up the cable by absolute frequency and temperature change relative to the 6 Apr 2016 11:00am scan show similar patterning for measurements; note that the Brugg cable has a "bulkhead termination," meaning the fibers are spliced Red-Green and Blue-Yellow to pass down and up the shaft within one cable body.

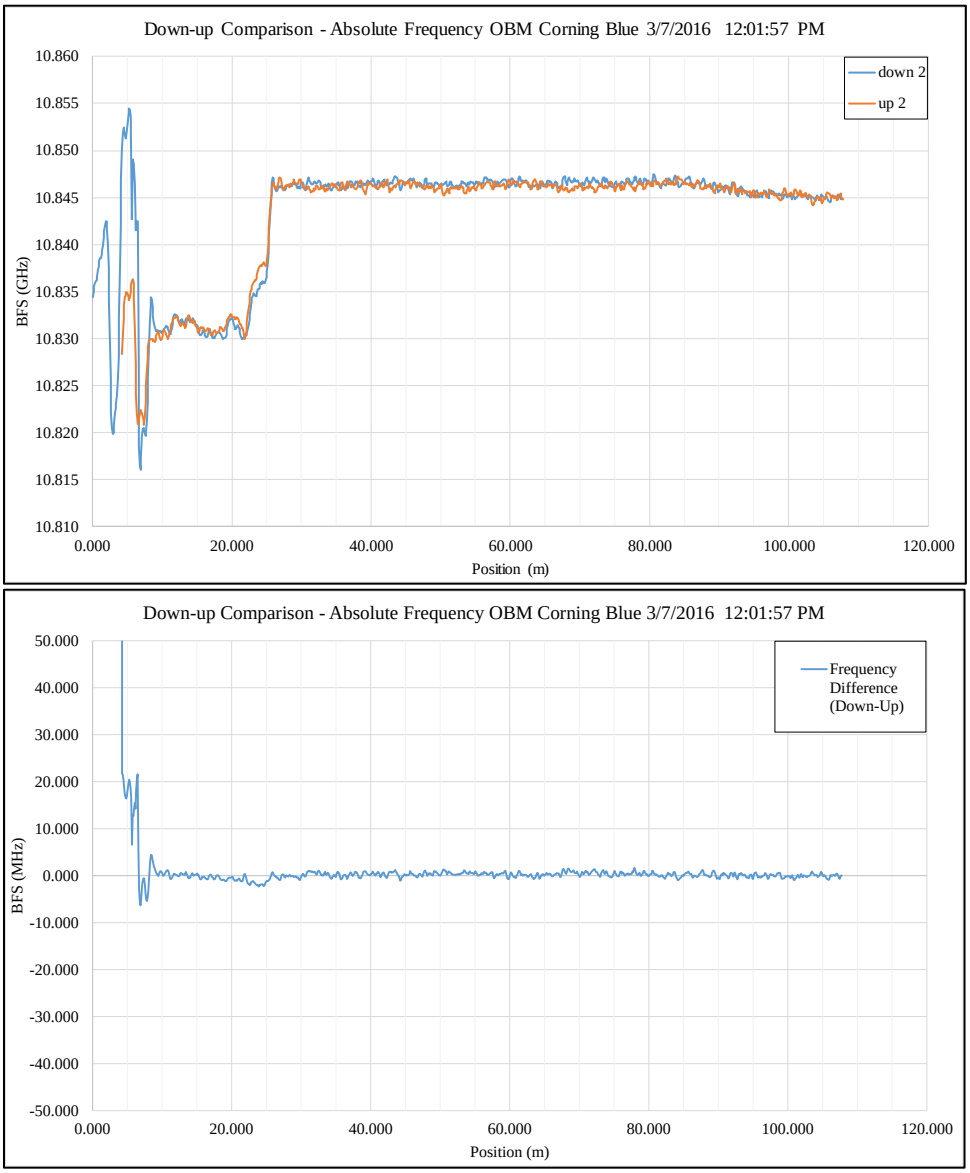

Figure 22: Corning Blue OBM temperature measurements compared down and up the cable by absolute frequency, and temperature change relative to the 6 Apr 2016 11:00am scan. Note, the Corning cable is in a looped configuration where the fibers do not pass back up the same cable sheath as going down, so the cable may not experience identical temperature/deployment phenomena.

Conclusions and Future Work

Linear regression analyses demonstrated strong correlation values R-squared coefficients greater than 0.990 with an average RMSE of ±0.8°F. Relationship coefficients defined the BFS dependence on sensor temperature. The DITEST caused BFS variations during sensor equilibrium (approximated by stable temp +/- 0.3°F). Both TidBit equilibration times and the stability interval were greater than 60-seconds, achieving 83% stability using 60-second measurement intervals.

Monitoring in the Orphan Boy Mineshaft during the February-July 2016 period demonstrated significant temperature variation over the May-June interval. Relative data analysis

methods used a baseline scan as a reference in order to remove manufacturing defect induced BFS textures in the temperature profiles. Thermal variations captured by the DST system were part of a scheduled test of the GHES, running first in heating mode (heat withdrawal) then in cooling mode (heat deposit). Significant temperature decreases were detected at 65m depth in the OBM in the depth profiles examined from the GHES test in May; further examination of OBM temperatures may yield more information.

Future work

Potential future work could include the following:

- Confirm fiber-optic measurements in the OBM with a deployment of TidBits for validation
- Perform new calibrations, changing the cable orientation in the calibration bath to examine the effects of different orientations on residuals and RMSE values
- Request operation of the GHES to examine effects on water temperature at depth
- Develop a method to remove manufacturing-induced frequency variations using more complex analysis calculations
    - Derive a true "absolute temperature" linear parameter set after resolving manufacturing errors
- Deploy new sensors in the OBM to determine if the current attachment methods are causing any frequency modulation

Acknowledgements

This material is based upon work supported by the National Institute for Occupational Safety and Health division of the Centers for Disease Control, specifically the Office of Mine Safety and Health Research, Contract number 211-2014-59580. Special thanks to Mary MacLaughlin of Montana Tech, for bringing me into the fold on this project. To Thomas Coleman of Silixa Ltd. for consulting on splicing and calibration procedures. Thank you to Larry Smith, Chris Gammons, and Scott Rosenthal, for driving me to grow as a technical writer. To Scott Rosenthal and the Mining Museum for mine access and UMEC diagrams. Thank you to Calvin Kammerer and Steve Berry, without whom we never would have reached full deployment depth in the Orphan Boy Mineshaft.

Personally, I would like to thank Logan Ward, for providing feedback and late-night editing tips. Lastly, thank you to my parents Greg and Andrea, for your moral and caffeinated support.

References

Aminossadati, S.; Mohammed, N.; and Shemshad, J. "Distributed Temperature Measurements using Optical Fibre [sic] Technology in an Underground Mine Environment." *Tunneling and Underground Space Technology.* Volume 25, Issue 3: p. 220-229. 2010.

Bao, X.; Webb, D.J.; and Jackson, D.A. "32-km distributed temperature sensor based on Brillouin loss in an optical fiber." *Optics Letters.* Volume 18, Issue 18: p. 1561-1563. 1993.

Bolognini, G. and Hartog, A. "Raman-based fibre sensors: Trends and applications." *Optical Fiber Technology.* Volume 19, Issue 6, Part B: p.678-688. 2013.

Boughton, D. A.; Hatch, C.; and Mora, E.; "Identifying distinct thermal components of a creek." *Water Resources Research.* Volume 48, Issue 9. 2012.

Gammons C. H.; Snyder D. M.; Poulson S. R.; and Petritz, K. "Geochemistry and stable isotopes of the flooded underground mine workings of Butte, Montana." *Economic Geology.* Volume 104, Issue 8: p. 1213-1234. 2009.

Glisic, B. and Inaudi, D. "Fibre Optic Methods for Structural Health Monitoring." *John Wiley & Sons.* 2008.

Hagan, T. "Temperature and Pressure Sensing in Three Flooded Underground Mine Workings in Butte, Montana, USA." Montana Tech Commons. 2015.

Hausner, M. B.; Wilson, K. P.; Gaines, D. B.; Suárez, F.; and Tyler, S. W. "The shallow thermal regime of Devils Hole, Death Valley National Park." *Limnology and Oceanography: Fluids and Environments*. Volume 3, Issue 1: p. 119-138. 2013.

Hurtig, E.; Grosswig, S.; and Kühn, K. "Distributed Fibre [Sic] Optic Temperature Sensing: A New Tool for Long-Term and Short-Term Temperature Monitoring in Boreholes." *Energy Sources.* Volume 19, Issue 1: p. 55-62. Print. 1997

Kurashima, T.; Horiguchi, T.; and Tateda, M. "Distributed-temperature sensing using stimulated Brillouin scattering in optical silica fibers." *Optics Letters.* Volume 15, Issue 8: 1038-1040. 1990.

Mizuno, Y.; Hayashi, N.; Tanaka, H.; Wada, Y.; Nakamura, K. "Brillouin scattering in multi-core optical fibers for sensing applications." *Scientific reports.* Volume 5. 2015.

Perez-Herrera, R. A. and Lopez-Amo, M. "Fiber optic sensor networks." *Optical Fiber Technology.* Volume 19, Issue 6: 689-699. 2013.

Ruffin, A B. "Stimulated Brillouin Scattering: An Overview of Measurements, System Impairments, and Applications." *Technical Digest: Symposium of Optical Fiber Measurements*. P. 23-28. 2004.

Selker, J. S.; Thevenaz, L.; Huwald, H.; Mallet, A.; Luxemburg, W.; Van de Giesen, N.; Stejskal, M.; Zeman, J.; Westhoff, M.; Parlange, M. B.; "Distributed fiber-optic temperature sensing for hydrologic systems." *Water Resources Research.* Volume 42, Issue 12. 2006.

Signorini, A.; Faralli, S.; Soto, M. A.; Sacchi, G.; Baronti, F.; Barsacchi, R.; Lazzeri, A. "40 km long-range Raman-based distributed temperature sensor with meter-scale spatial resolution." *Optical Fiber Communication Conference*. Optical Society of America, 2010.

Tyler, S. W.; Holland, D. M.; Zagorodnov, V.; Stern, A. A.; Sladek, C.; Kobs, S.; and Bryenton, J. "Using distributed temperature sensors to monitor an Antarctic ice shelf and sub-ice-shelf cavity." *Journal of Glaciology*. Volume 59, Issue 215: p. 583-591. 2013.

User Manual (UM-018) for Omnisens, DITEST STA-R. Tolochenaz: Omnisens SA [Switzerland] (2009).
User Manual (10385-G MAN-UTBI-001) for Onset, TidBit v2 UTBI-001. Cape Cod, Massachusetts: Onset. 2013.
User Manual (Document #400045-300) for SensorTran, Astra5k Raman DTS. Houston, Texas: SensorTran. 2009.
Zhou, D.; Li, W.; Chen, L.; and Bao, X. "Distributed temperature and strain discrimination with stimulated Brillouin scattering and Rayleigh backscatter in an optical fiber." *Sensors*. Volume 13, Issue 2: p. 1836-1845. 2013.

Appendix I: Splicing Guide

Universal splicing steps and tips

1. Strip the cable sheath from the inner cable components
2. Remove intermediate components that obstruct access to the fibers
3. Strip fiber of cladding material
4. Place a splice protector on the cladded fiber of one side of the fiber set to be spliced
5. Clean fiber with optical solution and optical wipes
6. Cleave with the base of the bare fiber @ #16 - #18 hash mark on the precision cleaver
7. Carefully remove fiber from cleaver
8. Place the fiber into the fusion splicer, with the cleaved end close to the fusion needle
9. Close the magnetic clasps on the stage with the cleaned and cleaved fiber
10. Close the stage-cover door
11. Initiate automated splicing sequence
12. Repeat steps 1-9, skipping step 4, as needed

Lead-In / Termination Cable / OCC / Corning

1. Slide vinyl tubing onto cable with heat-shrink (if applicable)
2. Strip sheath
3. Remove intermediate components
4. Place splice protector over fiber
5. Strip fiber
6. Clean fiber
7. Cleave @ #16 - #18 hash mark
8. Carefully remove fiber from cleaver
9. Place into fusion splicer
10. Press “Set” on fusion splicer
11. Allow splice, shut off after dB Loss reported
12. Open and open all latches and one side of the cable gate
13. While gently tensioning free bare fiber end, lift opposite cable gate
14. Slide splice protector over bare fiber, place carefully into the heat slot
15. Close and turn on fusion splicer, press “Heat”
16. Wait until 30s [minimum] after heater beeps its “completed cycle” tone
17. Remove spliced end, continue splicing fibers or slide vinyl tubing over splice and use a heat gun to shrink the heat-shrink down over the cable, washing the heat over (not holding the heat gun over one spot)
18. Run calibration scan on sensor to ensure splice integrity

Common Measurements

- Stripped cable – 4-5”
- Vinyl tubing – 8-12” (extra tube length is acceptable; inadequate tube length requires re-splicing)

Brugg Brusens V9

1. Be patient—this cable is very tough to splice because of the tension introduced by the metallic armoring layers
2. Use a razor to cut to the internal cable core around the circumference of the cable, 1” at a time until reaching 4-5”
3. Place the blade of a pair of wire cutters in the notch cut by the razor
4. Pull the cable and wire cutters in different directions to strip the section of sheath

5. Complete the splice as with the termination cable instructions

Brugg Brusteel / Temperature-85 (T-85)

1. Wrap the outer cable sheath 6" from the end in masking tape to a thickness of 1/4 – 3/8", creating a grip stop on the cable
2. Strip 4-5" of the outer cable sheath using a utility knife held in a reverse chest grip, keeping the cable on the table—take your time and don't try to strip off more than a quarter of the total sheath circumference at a time.
3. Carefully unwind the steel strength member fibers from the cable core tube
4. Collect steel fibers into a cluster
5. Tape the steel fibers nearest to the end of the cable, then use heavy-duty wire cutters to clip them near the base of the stripped section, 2-3 fibers at a time
6. Perform splices with isolated silica fibers

Common mistakes

1. Rushing to get the splice done
2. Forgetting to put the splice protector on one of the fibers before the bare fibers are spliced, requiring the splice to be clipped in order to install the splice protector
3. Forgetting to place heat shrink on vinyl tubing before bare splice is complete
4. Cutting the vinyl tubing too short
5. Not stripping enough cable to allow easy access to the fiber
6. Not leaving enough length in the fiber to allow multi-fiber cable splices to be performed (causes over-bending and introduces the possibility of bending beyond the minimum bend radius)
7. Failing to collect fiber remnants from the cleaver
8. Failing to turn off the fusion splicer after the splice is complete to prevent automated pylon separation during system reset, causing fiber straining and splice breaks
9. After each cleave, not resetting the cleaver **before** reloading with another fiber
10. Snapping the fiber by closing the cleaver without holding the fiber in place
11. Trying to run fusion splicer on "DC" setting when plugged into AC-power

Appendix II: Fiber-optic cable specifications

Technical specification information for fiber-optic cables used in this project were included as available in this section.

Brusens temperature 85°C

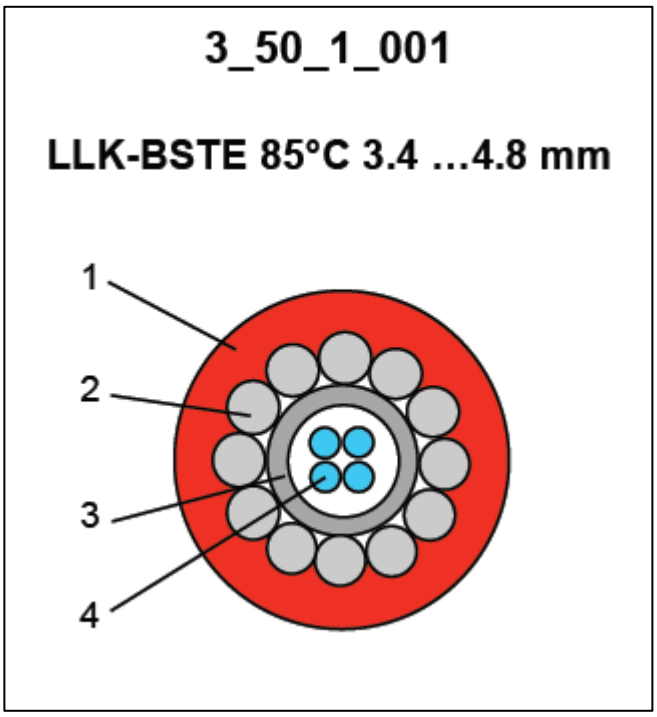

Figure A-1: Small fiber-optic temperature sensing cable, armored with stainless steel loose tube, stainless steel strength members and PA outer sheath, fast thermal response, for up to 8 fibers; (1) PA outer sheath; (2) Stainless steel wires, 316L; (3) Stainless steel loose tube, 316L; (4) Bend insensitive optical fibers with dual layer acrylate coating for increased micro bending performance

Description

- Gel filled central metal loose tube with up to 8 fibers, hermetically sealed
- High tensile strength
- High crush resistance
- Excellent rodent protection
- Laterally watertight
- High chemical resistance
- Robust abrasion resistant cable sheath
- Compact, high flexibility, small bending radius
- Halogen free
- Fast temperature response

Applications

- Sensing applications: e.g. temperature monitoring
- Sensing technologies: Raman, Brillouin, FBG etc.
- Harsh environment, outdoors

- Deployment in conduits, directly in the ground or attached to structures
- Connection and communication cable for sensing
- Temperature compensation cable for Brillouin

Standard optical fiber

- Multimode fiber: ITU-T G.651, 50µm or 62.5µm
- Single-mode fiber: ITU-T G.652.D or G.657
- Other fiber types and fiber quality

Temperature range

- Operating temperature: -40° C … + 85° C
- Storage temperature: -40° C … + 85° C
- Installation temperature: -10° C … + 50° C
- Short- term temperature: (max 60min) -50° C … +150° C

Cable sheath color

- Red, similar RAL 3000
- Other colors upon request

Standards

- Cable tests complying with IEC 60794-1-2

Remarks

- Fiber colors: 1 red, 2 green, 3 yellow, 4 blue,
- Other cable designs and temperature ranges available
- Standard cable marking with meter marks, special labeling of outer sheath upon request
- Accessories such as loops, fan-outs, connectors, mounting brackets etc. available
- Deployment training upon request
- For improved UV resistance, black cable sheath available upon request

Technical data:

Type	Max. no. of fibres units	Cable ø mm	Weight kg/km	Max. crush res. N/cm	Max. tensile strength installation N	Max. tensile strength operation N
1F	1	3.4	18	2000	800	600
2F	2	3.8	26	800	1500	1000
4F	4	3.8	26	800	1500	1000
8F	8	4.8	46	1000	3000	2000

Type	Min. bending radius with tensile mm	Min. bending radius without tensile mm	Hydrostatic pressure resistance x100kPa (bar)
1F…8F	20xD	15xD	300

Optical fiber data (cabled) at 20°C

Fiber Type	Attenuation, dB/km 850 nm	Attenuation, dB/km 1300 / 1310 nm	Attenuation, dB/km 1550 nm	Modal Bandwidth, MHz·km 850 nm	Modal Bandwidth, MHz·km 1300 nm
MMF 50/125	≤3.0	≤1.0	NA	700	500
MMF 62.5/125	≤3.5	≤1.0	NA	200	500
SMF	NA	≤0.36	≤0.25	NA	NA

Corning FREEDOM® LST™ Cable

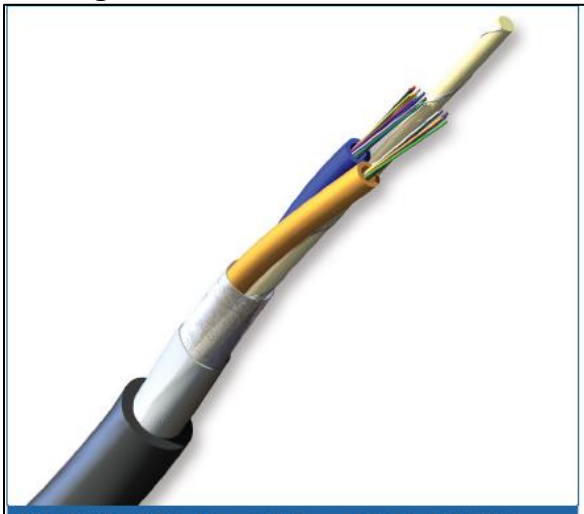

FREEDM LST Cables, 24 Fibers | Photo PIM0767

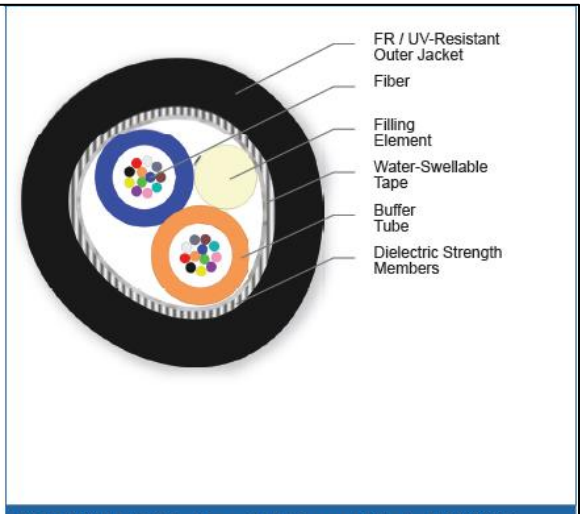

FREEDM LST Cables, 24 Fibers | Photo PIM1667

Temperature Range	
Storage	-40 °C to 70 °C (-40 °F to 158 °F)
Installation	-10 °C to 60 °C (14 °F to 140 °F)
Operation	-40 °C to 70 °C (-40 °F to 158 °F)

** Note: Corning recommends storing indoor/outdoor cable in a proper temperature environment prior to installation to allow the cable temperature to meet installation temperature range specifications for best installation results.*

Mechanical Characteristics Cable

Fiber Count	Product Type	Number of Tube Positions	Number of Active Tubes	Weight	Nominal Outer Diameter	Min. Bend Radius Installation	Min. Bend Radius Operation
2	Dielectric	1	1	56 kg/km (38 lb/1000 ft)	7.4 mm (0.29 in)	111 mm (4.4 in)	37 mm (1.5 in)
18 - 24	Dielectric	2	2 - 2	78 kg/km (53 lb/1000 ft)	9.7 mm (0.38 in)	146 mm (5.7 in)	97 mm (3.8 in)
6 - 12	Dielectric	1	1 - 1	56 kg/km (38 lb/1000 ft)	7.4 mm (0.29 in)	111 mm (4.4 in)	37 mm (1.5 in)

Transmission Performance

Multimode					
Fiber Core Diameter (µm)	62.5	50	50	50	50
Fiber Category	OM1	OM2	OM3	OM4	OM4 Extended Distance
Fiber Code	K	T	T	T	T
Performance Option Code	30	31	80	90	91
Wavelengths (nm)	850/1300	850/1300	850/1300	850/1300	850/1300
Maximum Attenuation (dB/km)	3.4/1.0	3.0/1.0	3.0/1.0	3.0/1.0	3.0/1.0
Serial 1 Gigabit Ethernet (m)	300/550	750/500	1000/600	1100/600	1100/600
Serial 10 Gigabit Ethernet (m)	33/-	150/-	300/-	550/-	600/-
Min. Overfilled Launch (OFL) Bandwidth (MHz*km)	200/500	700/500	1500/500	3500/500	3500/500
Minimum Effective Modal Bandwidth (EMB) (MHz*km)	220/-	950/-	2000/-	4700/-	5350/-

Notes: 1) *Improved attenuation and bandwidth options available.*
2) *Bend-insensitive single-mode fibers available on request.*
3) *Contact a Corning Customer Care Representative for additional information.*
4) *50 µm multimode fiber macrobend loss ≤ 0.2 dB at 850 nm for two turns around 7.5 mm radius mandrel.*

Single-mode		
Fiber Name	Single-mode (OS2)	Single-mode (OS2)
Fiber Category	G.652.D	G.652.D/G.657.A1
Fiber Code	E	H
Performance Option Code	01	01
Wavelengths (nm)	1310/1383/1550	1310/1383/1550
Maximum Attenuation (dB/km)	0.4/0.4/0.3	0.4/0.4/0.3

The Light Connection (TLC) single-mode simplex loose-tube cable

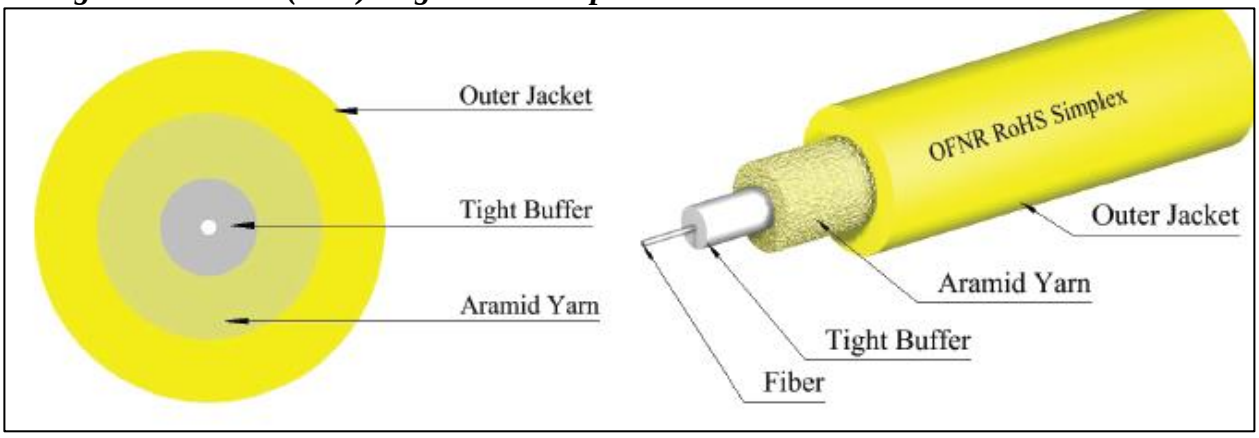

Figure A-2: The cross-section of TLC Simplex single-mode fiber, commonly referred to throughout this thesis as telecom cable or lead-in cable; the cable is of loose tube design, which allows for easier splicing and lower responses to strain from deployment and spooling. The cable used for this project is 2.95mm nominal OD with a bend radius of 7.5mm.

Applications

- Riser
- Plenum

Features

- 3mm, 2mm, 1.8mm and 1.6mm OD sizes to meet all patch cord applications
- Consistent 3.5lbs – 5lbs pull force for ease of buffer stripping
- Available in custom colors

Mechanical and Environmental Performance

OFNR	
Storage Temp	-40/ +70°C
Operating Temp	-20/ +70°C

	Part Number	Cable Rating	Nominal Diameter mm	Fiber Count	Weight lbs/km	Bend Radius
3.0mm	S09SX01CZNPY	OFNP	2.95	1	20	10 mm
	S09SX01CZNRY	OFNR	2.95	1	17	10 mm
	M62SX01C3NPO	OFNP	2.95	1	20	10 mm
	M62SX01C3NRO	OFNR	2.95	1	17	10 mm
	M50SX01CGNPA	OFNP	2.95	1	20	7.5 mm
	M50SX01CGNRA	OFNR	2.95	1	17	7.5 mm
	M50SX01C2NPO	OFNP	2.95	1	20	7.5 mm
	M50SX01C2NRO	OFNR	2.95	1	17	7.5 mm
	M50SX01C4NPA	OFNP	2.95	1	20	7.5 mm
	M50SX01C4NRA	OFNR	2.95	1	17	7.5 mm

Appendix III: Annotated Bibliography

The following studies are color-coded as to their primary use in the literature review. I have broken the literature down into smaller categories than used in the main text body to provide more information.

Calibration/Validation, Case Study/Proof of Concept, Theoretical background, Benchmarks for Accuracy, Site History

Aminossadati, S.; Mohammed, N.; and Shemshad, J. "Distributed Temperature Measurements using Optical Fibre Technology in an Underground Mine Environment." *Tunneling and Underground Space Technology.* Volume 25, Issue 3: p. 220-229. 2010.

This article reviewed a Raman sensing system for the purpose of mine air-temperature monitoring. I think one of the key points with this study was highlighting accuracy as a function of scan duration, primarily because ventilation monitoring is notorious for rapid changes in temperature. Aminossadati et al. validated measured temperatures using a Nova-sina digital temperature probe (model information not included, some models capable of 0.0001ºF accuracy), but did not mention how time matching between optical and digital measurements was accomplished. Spatial resolutions were reported as 1 m and 1°C.

Bao, X.; Webb, D.J.; and Jackson, D.A. "32-km distributed temperature sensor based on Brillouin loss in an optical fiber." *Optics Letters.* Volume 18, Issue 18: p. 1561-1563. 1993.

This article addresses the limited fiber-optic sensing technology of the 1990's, reviewing the electrical and optical engineering requirements to achieve better resolution. Resolutions detailed by Bao et al. were on the order of 5m with temperature resolutions of ± 1°C. Bao did explain that there are 9 splices over the length of the 32km long fiber; a calibrated sensor used Brillouin loss, not gain, in order to measure temperature. The results were consistent with using gain, but from what I gather, the electronics of the day could not cope with capturing gain (amplification of the signal due to the medium), but traditionally used loss (energy lost due to scattering). Bao did not explain loss (amplitude/intensity domain) in terms of how it is interpreted in Brillouin measurements (frequency domain).

Bolognini, G. and Hartog, A. "Raman-based fibre sensors: Trends and applications." *Optical Fiber Technology.* Volume 19, Issue 6, Part B: p.678-688. 2013.

This article is the only text I've found to succinctly describe and compare fiber-optic systems that use a single-stranded and looped configuration, contrasting their uses and potential accuracies. The article is general, but gives the best description of what a distributed sensor is. Bolognini et al. state "A distributed sensor could be considered as a multiplexed array of discrete point sensors and the metrology of the system described from that of each individual point."

Boughton, D. A.; Hatch, C.; and Mora, E.; "Identifying distinct thermal components of a creek." *Water Resources Research.* Volume 48, Issue 9. 2012.

Temperature patterns and textures were described for the first time (in the fiber-optic literature) in this article. This article described how the thermal stability of water requires significant spatial and temporal resolution to capture heat influx/outflow, especially when using temperature as a marker for groundwater path changes. The statistical methods used were beyond non-PhD students, or at the very least beyond someone not rigorously trained in statistics (such as I). Temperatures were measured at 2m intervals over a distance of 1km, **calibrated with an ice-water bath and a temperature logger** (at one position/small cable section, details are not given). **Onset pendant-style temperature loggers were used in this study (possibly the same model as I used).**

Gammons C. H.; Snyder D. M.; Poulson S. R.; and Petritz, K. "Geochemistry and stable isotopes of the flooded underground mine workings of Butte, Montana." *Economic Geology*. Volume 104, Issue 8: p. 1213-1234. 2009.

This article was primarily used as a site history document, as no spatially continuous time-series data exists to the best of my knowledge. Gammons et al. discussed how reduction reactions may lead to hydrothermal gradients where there would not be one otherwise; hydrothermal controls on alteration and mineral transport would be a good target for a monitoring system. They noted "Direct evidence of vertical circulation in the Anselmo mine-shaft was noted, via a submersible movie camera, by MBMG hydrogeologists in 2005. When the movie camera was held stationary, suspended particles in the water column were clearly shown to be moving upwards through the shaft (Mike Kerschen, MBMG, Personal Communication, 2007)."

Glisic, B. and Inaudi, D. "Fibre Optic Methods for Structural Health Monitoring." *John Wiley & Sons*. 2008.

The use of long gauge (distributed) sensors comes into its own when monitoring on multiple spatial levels – it allows for the characterization of localized phenomena while preserving changing conditions throughout the structure. Common structures (bridges, roads, support columns, dams) collapse only after significant malfunction over a long period of time, so long term monitoring is important. The portion of the book that I read detailed how to scale temporal resolution to characterize variable changes in different time-scales. For example, looking at the progression of a surface crack as it begins to extend to depth, or how daily temperature variations are missed when looking at hourly or monthly patterns. Decoupling was the other important factor, deploying sensors side-by-side to separate changes induced by temperature from those caused by pressure or attachment methods, as in instrumenting a flooded mineshaft to great depth.

Hagan, T. "Temperature and Pressure Sensing in Three Flooded Underground Mine Workings in Butte, Montana, USA." Montana Tech Commons. 2015.

The previous study performed in the OBM highlighted important steps for temperature validation using the TidBits, namely to avoid hysteresis by leaving the TidBits at depth. Looking at temperature as a function of depth is a good reminder of the uses of the technology. Future work may include deployments in other mineshafts to create a library of spatially-continuous time-series data.

Hausner, M. B.; Wilson, K. P.; Gaines, D. B.; Suárez, F.; and Tyler, S. W. “The shallow thermal regime of Devils Hole, Death Valley National Park.” *Limnology and Oceanography: Fluids and Environments*. Volume 3, Issue 1: p. 119-138. 2013.
The authors used a looped configuration with a constant calibration bath method common in Raman monitoring, using the amplitude measured at two different temperatures to create a linear relationship function from the two points. The study used the RMSE method, a residual analysis calculation, for determining the cable sensor accuracy. Increased spatial resolution is obtainable through calculated manipulation and overlap of sensor cable coils, with low standard deviations at ± 0.6°C, largely due to the overlap of measurements by sensor geometry.

Hurtig, E.; Grosswig, S.; and Kühn, K. "Distributed Fibre [Sic] Optic Temperature Sensing: A New Tool for Long-Term and Short-Term Temperature Monitoring in Boreholes." *Energy Sources.* Volume 19, Issue 1: p. 55-62. Print. 1997
This article was primarily used Optical absorption for fiber lengths greater than 8km decreases available space and time resolution. Reported accuracies were ± 0.3K, using spatial resolutions of 1m. Light-pulse durations were 10ns, an order of magnitude longer than what was used by the project’s DITEST. While this reduces temporal and spatial resolution (considering spatial resolution was already defined), longer scans and longer pulse durations ultimately resolves fine-grained temperature profiles better than shorter scans—it’s a matter of prioritizing what measurement characteristics (accuracy, temporal/spatial resolution, scan scheduling, etc.) are important. The authors point out “The fibre [sic] optic temperature sensing should be used especially for on-line and long-term surveying the temperature field and its variations with time rather than for simple borehole logging.”

Kurashima, T.; Horiguchi, T.; and Tateda, M. "Distributed-temperature sensing using stimulated Brillouin scattering in optical silica fibers." *Optics Letters.* Volume 15, Issue 8: 1038-1040. 1990.
This was the oldest relevant article that spoke of fiber-optic sensing as a potential sensor system once technology caught up with the theory. Calibration slopes were on the order of 1.25MHz/°C but were not detailed as to their setup or how data analysis was performed. Reported temperature resolutions were 3°C, with a spatial resolution of 100m along a 1.2km cable.

Mizuno, Y.; Hayashi, N.; Tanaka, H.; Wada, Y.; Nakamura, K. "Brillouin scattering in multi-core optical fibers for sensing applications." *Scientific reports.* Volume 5. 2015.
This article targeted a multi-fiber cable in both strain and temperature calibrations. The calibration setup was not detailed, but used Brillouin sensing methods to accomplish 1.00MHz/°C with variations of ±0.03MHz/°C. The authors focused on power outputs vs BFS, which provided another check on calibration reliability (this required technician-level knowledge of the signal interrogator).

Perez-Herrera, R. A. and Lopez-Amo, M. "Fiber optic sensor networks." *Optical Fiber Technology.* Volume 19, Issue 6: 689-699. 2013.

This article described the operational aspects of fiber-optic sensor networks, comparing sensing methods, sensor layouts, advantages and disadvantages of fiber sensors, and addressing the fragility of fiber-optic networks. The document provided a number of diagrams that, for me, illustrated the need for parallel-type sensor layout designs, as sensors in series would be useless if and when a singular sensor failed, especially for systems that use a looped or return-on-end (turn-around) style transmission paths. This is probably the most useful document for creating a pro/con list in favor of fiber sensors. Perez-Herrera and Lopez-Amo are to be commended for their use of diagrams—this is certainly one of the first documents I would recommend a new student or researcher reads before entering the field.

Ruffin, A B. "Stimulated Brillouin Scattering: An Overview of Measurements, System Impairments, and Applications." *Technical Digest: Symposium of Optical Fiber Measurements*. P. 23-28. 2004.

Ruffin's article was more of an academic article describing the technical process of instigating and detecting Brillouin scattering events. The article explained optical power when present in a fiber and clarified what the Brillouin gain spectrum refers to in terms of phase-shifting light from stimulated Brillouin scattering events. Much of the information presented is not practically useful for this project, as it relates to the calculation of Brillouin scattering events from electro-optical interpretations (this would be useful for someone with more electrical/optical engineering experience).

Selker, J. S.; Thevenaz, L.; Huwald, H.; Mallet, A.; Luxemburg, W.; Van de Giesen, N.; Stejskal, M.; Zeman, J.; Westhoff, M.; Parlange, M. B.; "Distributed fiber-optic temperature sensing for hydrologic systems." *Water Resources Research.* Volume 42, Issue 12. 2006.

New researchers on the project should read this document first, it reviews the technology, accuracy, and uses for fiber-optic sensors in a succinct manner. This is a great introductory document. The article provides good sources for understanding theory in the fiber-optic sensor research area, as it is a review of past research and the direction of the field. The best point the authors make is, "There are trade-offs between precision in temperature, temporal resolution, and spatial resolution, following the square root of the number of measurements made; thus brief, short measurements are less precise than measurements taken over longer spans in time and space."

Signorini, A.; Faralli, S.; Soto, M. A.; Sacchi, G.; Baronti, F.; Barsacchi, R.; Lazzeri, A. "40 km long-range Raman-based distributed temperature sensor with meter-scale spatial resolution." *Optical Fiber Communication Conference*. Optical Society of America, 2010.

Signorini et al. pointed out Raman systems are limited by optical budget because they rely on measurements in the intensity; useful for another case-study in fiber-optic sensors, but not for manipulating or calibrating our Brillouin-based system. Demonstrated long-range limitations of temperature accuracy with changing temporal resolutions over distance for Raman-based systems.

Tyler, S. W.; Holland, D. M.; Zagorodnov, V.; Stern, A. A.; Sladek, C.; Kobs, S.; and Bryenton, J. “Using distributed temperature sensors to monitor an Antarctic ice shelf and sub-ice-shelf cavity.” *Journal of Glaciology*. Volume 59, Issue 215: p. 583-591. 2013.
This study was used as an example of field deployments of fiber-optic sensors. Brugg temperature sensing cable with a bulkhead turnaround (mirror-on-end attachment that allows signal to pass down one fiber and back up another in the same cable body) was utilized for the Raman sensing system. A calibration bath of unknown size and unknown process was used for calibration, presumably like other dual-temperature systems.

User Manual (UM-018) for Omnisens, DITEST STA-R. Tolochenaz: Omnisens SA [Switzerland] (2009).
According to the DITEST user manual, calibrations should be conducted for two thermal regimes if applicable to the measurement needs, namely for areas that will experience both 0-20°C and 20-85°C. The manual does not recommend any methods beyond the temperature ranges.

User Manual (10385-G MAN-UTBI-001) for Onset, TidBit v2 UTBI-001. Cape Cod, Massachusetts: Onset. 2013.
This document provided operational parameters for the TidBits, primarily accuracy, precision, and the functional temperature range.

User Manual (Document #400045-300) for SensorTran, Astra5k Raman DTS. Houston, Texas: SensorTran. 2009.
This manual was from a Raman-based DTS system owned by a partner group of the project. The system used a drag-and-drop style calibration to scale the intensity separation to the temperature difference between two different temperature calibration baths, in which a small coil of cable was placed.

Zhou, D.; Li, W.; Chen, L.; and Bao, X. "Distributed temperature and strain discrimination with stimulated Brillouin scattering and Rayleigh backscatter in an optical fiber." *Sensors*. Volume 13, Issue 2: p. 1836-1845. 2013.
The authors used specially doped fiber sensors to achieve the high accuracy; without differing types of fibers, the accuracy was reduced to 4°C, which is not very useful. An experimental accuracy of ±1.2°F and 0.50m spatial resolution were determined capable using Brillouin methods. The spatial resolution was determined by the pulse width difference between pump and probe pulses, NOT by time-response calculations based on fiber index and delay using the speed of light as in other Brillouin interrogators.